Dissolution of Lead- and Lead-Arsenic-Jarosites at pH 2 and 8 and 20°C: Insights from Batch Experiments

ADRIAN M. L. SMITH[1,2,3,4], WILLIAM E. DUBBIN[1], KATE WRIGHT[2,5], AND KAREN A. HUDSON-EDWARDS[3*]

[1] Department of Mineralogy, The Natural History Museum, Cromwell Road, London, SW7 5BD, UK.

[2] Davy Faraday Research Laboratory, The Royal Institution of Great Britain, 21 Albemarle Street, London, W1S 4BS, UK.

[3] Research School of Earth Sciences at UCL-Birkbeck, Birkbeck, University of London, Malet Street, London, WC1E 7HX, UK.

[4] Now at Entec UK Ltd, Canon Court North, Abbey Lawn, Abbey Foregate, Shrewsbury, SY2 5DE, UK.

[5] Now at Nanochemistry Research Institute, Department of Applied Chemistry, Curtin University of Technology, GPO Box U1987, Perth, WA 6845.

*Corresponding author

Revised version re-submitted to: *Chemical Geology*

Date of re-submission: 10 October 2005

Keywords: Pb-jarosite, Pb-As-jarosite, Fe hydroxide, Pb sulphate, acid mine drainage, dissolution

Abstract

Lead- and Pb-As-jarosites are minerals common to acidic, sulphate-rich environments, including weathering zones of sulphide ore deposits and acid rock or acid mine drainage (ARD/AMD) sites, and often form on or near galena. The structures of these jarosites are based on linear tetrahedral-octahedral-tetrahedral (T-O-T) sheets, comprised of slightly distorted FeO_6 octahedra and SO_4^{2-} (-AsO_4^{3-} in Pb-As-jarosites) tetrahedra. To better understand the dissolution mechanisms and products of the break down of Pb- and Pb-As-jarosite, preliminary batch dissolution experiments were conducted on synthetic Pb- and Pb-As-jarosite at pH 2 and 20°C, to mimic environments affected by ARD/AMD, and at pH 8 and 20°C, to simulate ARD/AMD environments recently remediated with slaked lime ($Ca(OH)_2$). All four dissolutions are incongruent. Dissolution of Pb-jarosite at pH 2 yields aqueous Pb, Fe and SO_4^{2-}. The pH 8 Pb-jarosite dissolution yields aqueous Pb, SO_4^{2-} and poorly crystalline $Fe(OH)_3$, which does not appear to resorb Pb or SO_4^{2-}, possibly due to the low solution pH (3.44-3.54) at the end of the experiment. The pH 2 and 8 dissolutions of Pb-As-jarosite result in the formation of secondary compounds (poorly crystalline $PbSO_4$ for pH 2 dissolution; poorly crystalline $PbSO_4$ and $Fe(OH)_3$ for pH 8 dissolution), which may act as dissolution inhibitors after 250 to 300 h of dissolution. In the pH 2 dissolution, aqueous Fe, SO_4^{2-} and AsO_4^{3-} also form, and in the pH 8 dissolution, $Fe(OH)_3$ precipitates then subsequently resorbs aqueous AsO_4^{3-}. The dissolutions probably proceed by preferred dissolution of the A- and T-sites, which contain Pb, and SO_4^{2-} and AsO_4^{3-}, respectively, rather than Fe, which is sterically remote, within the T-O-T Pb- and Pb-As-jarosite structures. These data provide the foundation necessary for further, more detailed investigations into the dissolution of Pb- and Pb-As-jarosites.

1. INTRODUCTION

Lead and lead-arsenic jarosites are members of the isostructural jarosite-alunite group minerals that occur in the oxidized portions of sulphide ores, especially those rich in galena (Simons and Mapes, 1956; Dubinina and Kornilovich, 1959; Vasilevskaya, 1970; Roca *et al*., 1999), environments contaminated by acid rock or acid mine drainage (ARD/AMD) (Hochella et al., 1999; Hudson-Edwards *et al*., 1999; Rousel et al., 2000), and metallurgical wastes (Dutrizac, 1983; Crundwell and Bryson, 1992; Bigham and Nordstrom, 2000). The general formula of jarosite minerals is $AB_3(TO_4)_2(OH)_6$, where A represents cations with a coordination number greater than or equal to 9, and B and T correspond to cation sites with octahedral (O) and tetrahedral (T) coordination, respectively (Jambor, 1999; Hawthorne *et al*., 2000). In Pb-bearing jarosites, the B site cation is Fe(III) and the A site is occupied by both Pb(II) and H_3O^+ (Brophy and Sheridan, 1965; Kubisz, 1970; Dutrizac and Kaiman, 1976; Ripmeester *et al*., 1986) in 12-fold coordination. Iron deficiencies in the B site are expressed through the $Fe:SO_4$ molar ratio, which typically is significantly lower than the ideal of 3:2 (Kubisz, 1970; Alpers *et al*., 1989), with ratios as low as 2.33:2 (Ripmeester *et al*., 1986) and 2.20:2 to 2.57:2 (Härtig *et al*., 1984). These Fe deficiencies are charge balanced by the incorporation of water (as hydronium) into the jarosite structure (Kubisz, 1970; Härtig *et al*., 1984; Ripmeester *et al*., 1986; Alpers *et al*., 1989). The T site in most Pb-jarosites is occupied by SO_4^{2-}, whereas in Pb-As-jarosites, it is occupied by both SO_4^{2-} and AsO_4^{3-} (Kubisz, 1964; Brophy and Sheridan, 1965).

Lead- and Pb-As-jarosites have environmental relevance because they contain potentially toxic Pb and As in significant quantities, and thus, upon dissolution, may release these elements in bioavailable form to ecosystems. Only limited work has been carried out on the dissolution and stability of Pb- and Pb-As-jarosite (Patino *et al*., 1994, 1998; Vinals *et al*., 2003). Consequently, there are insufficient data upon which to assess the true environmental risk posed by these minerals. Recent studies on end-member K-jarosite showed that this mineral dissolves incongruently at pH 2 and 20°C to yield aqueous K, Fe and SO_4^{2-}, while dissolution at pH 8 and 20°C yields aqueous K

and SO_4^{2-} and goethite (Smith *et al*., 2005). This goethite did not, however, resorb any dissolved K or SO_4^{2-}. If Pb- and Pb-As-jarosite dissolve in a similar fashion, considerable amounts of aqueous Pb and As could be released to ARD/AMD and other environments, causing significant environmental harm. This paper reports the results of a preliminary study that monitors the dissolution and release of constituent elements (Pb, Fe, SO_4^{2-}, AsO_4^{3-}) from synthetic jarosites using batch dissolution experiments, characterizes new compound(s) formed as a result of these experiments, and determines whether resorption of Pb and As on these new compounds occurs.

2. METHODS AND MATERIALS

2.1. Synthesis of Pb- and Pb-As-jarosites

Pb-jarosite was synthesized using the methods of Dutrizac and Kaiman (1976) and Dutrizac *et al*. (1980), using a one L solution containing 0.054 M $Fe_2(SO_4)_3 \cdot 5H_2O$ and 0.01 M H_2SO_4, while Pb-As-jarosite was made following the method of Alcobe *et al*. (2001) from a 1 L solution containing 0.054 M $Fe_2(SO_4)_3 \cdot 5H_2O$ and 0.00946 M H_3AsO_4. In both cases, the solutions were subsequently placed in 2 L reaction vessels fitted with spiral condensers, then heated by means of a sand bath to 95ºC (1 atm) with constant stirring (400 rpm). When the solution temperatures reached 95ºC, 200 mL of 0.03 M $Pb(NO_3)_2$ (Aldrich) was added, with stirring, to each solution at a rate of 6 mL hr^{-1}. Once all the $Pb(NO_3)_2$ had been added, the precipitates were stirred (400 rpm) for a further 5 h, after which they were allowed to settle and the residual supernatant solutions decanted. The precipitates were then washed several times with ultrapure water (18 MΩ cm^{-1}) and dried at 110°C for 24 h.

2.2. Characterization of Synthetic Pb- and Pb-As-jarosites

The precipitation products were identified by crystallography using powder X-ray diffraction (XRD) analysis at 25°C with a Philips PW1050 vertical powder diffractometer utilizing Co $K\alpha_1 K\alpha_2$ ($\lambda\alpha_1$ = 1.788965 Å and $\lambda\alpha_2$ = 1.792850 Å) radiation at 35 kV and 30 mA. The 2-theta range was 5-155º, step size 0.025º and step time 10s. Unit cell parameters were calculated through Rietveld

refinement using GSAS (Larson and Von Dreele 1998) and the 'model free' Le Bail Method (Le Bail *et al*. 1988), where individual '$|F_{obs}|$' are obtained by Rietveld decomposition from arbitrarily identical values. In addition to the structure factors, free refinement was made of the lattice parameters constrained according to the rhombohedral symmetry of the space group in the centred hexagonal setting, background, profile parameters, and the instrumental zero-point. In all cases, a pseudo-voigt profile was used.

For quantitative total elemental analysis, approximately 60 mg of each of the two synthetic jarosites were dissolved in polypropylene beakers by adding concentrated HCl dropwise, with stirring, until no solid remained. The acidified solutions were then diluted to 50 mL with 2% HNO_3, and analysed for Pb, Fe, S and, in the case of the Pb-As-jarosite, As, by inductively coupled plasma optical emission spectrometry (ICP-OES) using a simultaneous solid-state detector (CCD) (Varian Vista-Pro, axial configuration). All analytical ICP-OES results were within one standard deviation of the mean.

Fourier transform infrared (FTIR) spectroscopy was used to characterize the vibrational modes within the synthetic jarosites. Spectra were collected with a PerkinElmer Spectrum One FTIR spectrometer using the KBr pellet (Ø13 mm) technique. The spectra (400 – 4000 cm^{-1}) were recorded in transmission mode immediately after pellet preparation. Five scans were accumulated, each with a resolution of 4 cm^{-1}.

Particle morphology was observed using scanning electron microscopy (SEM) at 5.0 to 10.0 kV accelerating voltage and a spot size of 2.0 to 3.0 μm (Philips XL30 FEG). Specific surface area was determined by nitrogen multipoint BET analysis (Brunauer et al., 1938) using a Micromeritics Gemini III 2375 surface area analyser.

2.3. Dissolution Experiments

Both acidic (pH 2.0) dissolution batch experiments, which mimic environments affected by ARD/AMD, and alkaline (pH 8.0) dissolution batch experiments, which mimic ARD/AMD

environments recently remediated with slaked lime ($Ca(OH)_2$), were carried out following the procedure of Baron and Palmer (1996). Briefly, for both sets of experiments, 100 mg of the two synthetic jarosites were suspended in 500 mL of ultrapure water (18 MΩ cm^{-1}). For the acid dissolution, the initial pH was set to 2.0 by the dropwise addition of concentrated $HClO_4$. For the alkali dissolution, the initial pH was adjusted to 8.0 by the incremental addition of 0.01 M $Ca(OH)_2$. Both the acid and alkaline dissolutions were conducted in triplicate, at 20°C and 1 atm, and were unbuffered, allowing free drift of pH. All pH measurements were obtained with an Accument AP50 meter equipped with a Russell Emerald combination electrode. The solutions were transferred to 750 mL acid washed Amber HDPE bottles, then agitated with a roller mixer (Stuart SRT2) operating at a fixed speed of 33 rpm.

Ten mL aliquots of the bulk solutions were obtained periodically by pipette while an overhead stirrer (~ 50 rpm) maintained a uniform suspension. Aliquots were filtered through 0.025 μm MF Millipore filters. A 4.5 mL aliquot of filtered sample was then acidified to make a 1% v/v HNO_3 matrix, which was subsequently analyzed for Pb_{tot}, Fe_{tot}, S_{tot} and As_{tot}. All S and As were assumed to be present as SO_4^{2-} and AsO_4^{3-}, respectively. The pH of the bulk solution was measured during each sampling episode. At the end of each dissolution experiment, the residual jarosite solids were recovered by filtration through a 0.22 μm MF Millipore filter, allowed to air dry at 20°C in a desiccator, then stored in an air-tight plastic vial.

The pH and concentrations of Pb_{tot}, Fe_{tot}, SO_{4tot} and AsO_{4tot} were used to calculate equilibrium aqueous activities of Pb^{2+}, Fe^{3+}, SO_4^{2-} and $H_2AsO_4^-$ with The Geochemist's Workbench (GWB, version 4.0.2) (Bethke, 1996). Activity coefficients and saturation indices were calculated using the extended form of the Debye-Hückel equation described by Helgeson (1969) and the latest form of the GWB thermodynamic database (based on the 1996 revision of the EQ3/6 database; Wolery, 1979, 1996). We calculate the activity of the arsenic oxyanion $H_2AsO_4^-$, rather than AsO_4^{3-} because, although the latter is a structural unit (T-site) in Pb-As-jarosites, it is not a stable aqueous

species under acidic (pH < 6.2), oxidising conditions (Smedley and Kinniburgh, 2002). Under the pH 8 dissolution conditions, $H_2AsO_4^-$ is the stable aqueous form of As(V).

The residual solids were identified by powder XRD analysis at 25ºC using a Siemens D500 diffractometer equipped with a scintillation counter. Tube operating conditions were 40 kV and 40 mA, with a secondary graphite monochromator used to select Cu Kα radiation (λ = 1.5418 Å). The 2-theta range was 10-70^o, step size 0.020^o and step time 27s. The residual solids were characterized further using quantitative wet chemical analysis, SEM and FTIR, as described above for the unaltered synthetic jarosites.

These batch experiments provide important, but largely preliminary insights into the dissolution of jarosites as they do not consider the effects of temperature, aqueous phase mixing rate, suspension density or the removal of reaction products on dissolution kinetics. Our data will nevertheless provide the necessary foundation for such experimental refinement, as exemplified previously for the systematic examination of calcite and anorthite dissolution (e.g., Rickard and Sjvberg, 1983; Sjvberg and Rickard, 1983; Amrhein and Suarez, 1992).

3. RESULTS

3.1. Characterization of Synthetic Pb- and Pb-As-Jarosites

The jarosite synthesis produced yellow precipitates with Munsell colours 10YR 6.5/7 (Pb-jarosite) and 10YR 8/8 (Pb-As-jarosite). Comparison of the powder X-ray diffraction patterns for Pb-jarosite and Pb-As-jarosite with those in the International Centre for Diffraction Data Powder Diffraction Files (ICDD PDF 39-1353 and 19-0689, respectively) suggested that all peaks arise from the structure of the plumbojarosite (Pb-jarosite) and beudantite (Pb-As-jarosite). The absence of additional peaks indicated that no other compounds were present at detectable levels (Fig. 1a, 2a). The calculated lattice parameters of the synthetic Pb-jarosite are a_0 = 7.3347(7) and c_0 = 16.9700(5), in contrast to the standard ICDD PDF file values (a_0 = 7.335(1); c_0 = 33.850(8). The c_0 value of the synthetic Pb-jarosite is one-half that of the corresponding ICDD PDF c_0 value, due to the better

goodness of fit (χ^2 values) achieved using a single, rather than a doubled, unit cell. No super lattice XRD reflections, which would indicate a doubled unit cell, were evident in the diffraction pattern for the synthetic Pb-jarosite (Fig. 1a). The calculated lattice parameters of the synthetic Pb-As-jarosite are a_0 = 7.3417(8) and c_0 = 16.9213(6), similar to the standard ICDD PDF file values (a_0 = 7.32; c_0 = 17.02).

Atomic percentages of the A-, B- and T-site elements were determined using the total elemental analysis data. In an end-member plumbojarosite structure, the theoretical Pb(II) occupancy in the A-site is set at 0.5 (thus, the A-site is charge-ordered), in comparison to the beudantite structure, which has full Pb(II) occupancy of 1.0. The formulas of the synthetic Pb- and Pb-As-jarosites, calculated using the modified formula of Kubisz (1970), are $(H_3O)_{0.74}Pb_{0.13}Fe_{2.92}(SO_4)_2(OH)_{5.76}(H_2O)_{0.24}$ and $(H_3O)_{0.68}Pb_{0.32}Fe_{2.86}(SO_4)_{1.69}(AsO_4)_{0.31}(OH)_{5.59}(H_2O)_{0.41}$, respectively. These formulas suggest that the synthetic jarosites produced are not true plumbojarosite nor beudantite, despite the fact that, crystallographically, their XRD patterns match those of these minerals. For this reason, we will continue to refer to the synthetic jarosites as 'Pb-jarosite' and 'Pb-As-jarosite'.

The FTIR spectra for the jarosites prepared in this study (Fig. 3a, 4a) are similar to those previously reported (Powers *et al*., 1975; Serna *et al*., 1986; Baron and Palmer, 1996; Drouet and Navrotsky 2003). The intense absorption observed in the region 2900 to 3700 cm^{-1} is attributed to O-H stretching (ν_{OH}). The band shift toward lower frequencies for Pb-jarosite (3352 cm^{-1}) and Pb-As-jarosite (3343 cm^{-1}), compared with end-member K-jarosite (3385 cm^{-1}) (Smith *et al*., 2005), is probably due to an increase in hydrogen bond energy within the structure of the former minerals (Powers *et al*., 1975; Drouet and Navrotsky, 2003). Sulfate oxygen atoms are located on trigonal axes, parallel to the c-axis of the unit cell, and are surrounded by three hydroxyl groups (Hendricks, 1937). It is therefore possible to distinguish two vibrational modes, O-H and H-OSO_3, around the hydrogen. The band observed at 1634 to 1641 cm^{-1} (Fig. 3a) is attributed to HOH deformation, in agreement with the results of others (Powers *et al*., 1975; Baron and Palmer, 1996; Drouet and

Navrotsky, 2003). Lead-As-jarosite has a relatively low ν_{OH} vibration frequency (i.e., 1634 cm^{-1}) due to the partial substitution of arsenate for sulfate (Fig. 4a); arsenate is represented in the spectra as two peaks at 813 and 855 cm^{-1} (these correspond to the $\nu_1(AsO_4^{3-})$ and $\nu_3(AsO_4^{3-})$ modes, respectively, Fig. 4a).

The Pb-jarosite crystals exhibit rhombohedral (pseudocubic) morphology typical of Pb-bearing jarosites (Dutrizac and Chen, 2003) (Fig. 5a), while the Pb-As-jarosite crystals are intergrown, with a pseudo-rhombohedral to globular morphology (Fig. 5b). The crystallites have diameters of 1-3 μm, with surface areas of 1.03 ± 0.023 and 9.58 ± 0.096 m^2g^{-1} for Pb-jarosite and Pb-As-jarosite, respectively.

3.2. Dissolution at pH 2

3.2.1. Solution Chemistry

For Pb-jarosite, most of the pH 2 dissolution occurred within the first 250 h, with dissolution rates declining rapidly after this time, and steady state conditions achieved after approximately 1500 h (Fig. 6a, b). The final aqueous Pb concentration was between 0.0108 and 0.0196 mmol L^{-1} (Table 1), and the pH remained nearly constant over the whole of the experiment ($pH_{initial}$ = 2.00, pH_{final} = 2.07). Molar ratios of ions in solution were calculated with respect to SO_4^{2-}, which is assigned a stoichiometric value of 2, a convention frequently used in calculating the molecular composition of jarosites (Baron and Palmer, 1996). The Pb:SO_4 molar ratio in solution varied from 0.109 – 0.112, and the Fe ratio varied from 2.79 – 2.83 (Table 1). Calculated equilibrium aqueous activities and saturation indices for the pH 2 dissolution are compiled in Tables 2 and 3, respectively. The charge balance error across the triplicates ranged from 3-5% (Table 2). Saturation indices for hematite and goethite were positive, and that for anglesite was negative (Table 3).

The element concentration profiles for the pH 2 dissolution of Pb-As-jarosite (Fig. 7) are considerably different from those for the pH 2 Pb-jarosite dissolution (Fig. 6). The Pb concentration in the former is extremely low, but even at this low concentration, one observes a sharp decrease

from about 0.00022 mmol L^{-1}, to a plateau of 0.00006 mmol L^{-1}, within the first 250 to 300 h of the experiments (Fig. 7b). The concentration of SO_4^{2-} also decreased sharply, to a minimum of 0.01175 mmol L^{-1} near 250 to 300 h, then increased in a roughly linear fashion from 300 to 1250 h (Fig. 7c), where it was similar to the concentration at the onset of the experiment. The shapes of the Fe and AsO_4^{3-} profiles are similar, with concentrations increasing rapidly to 250 h, after which each reached a plateau (Fig. 7a). Because it was difficult to determine the point of steady state for all ions, the experiments were terminated at 2250 h. For this reason, ion concentrations and pH values are reported as final, rather than steady state concentrations (Table 1). Molar ratios were again calculated with respect to SO_4^{2-}, which was assigned a stoichiometric value of 1.69, based on the composition of the synthetic Pb-As-jarosite. Lead, Fe and AsO_4^{3-} molar ratios in solution are 0.0040-0.0069, 8.485-8.713 and 4.741-4.849, respectively (Table 1). The charge balance error for The Geochemist's Workbench calculations (Table 2) was 5%, and saturation indices for hematite and goethite were positive (Table 3).

3.2.2. Residual Solids

Total element concentrations, and their molar ratios with respect to SO_4^{2-}, in residual solids from the three Pb-jarosite dissolutions, are summarized in Table 4. Once again, SO_4^{2-} is assigned, by convention, a stoichiometric value of 2. The Pb ratio in the residual solids varied from 0.230 – 0.236, while the Fe ratio varied from 3.133 – 3.147. The X-ray diffractograms and FTIR spectra for the pH 2 dissolution solids were both similar to those of the unaltered synthetic Pb-jarosite (compare Figs. 1a, 1b and 3a, 3b), with no extra peaks (XRD) or bands (FTIR) arising from additional compounds present. Moreover, neither micrograph in Figure 8 showed evidence of a new solid compound, consistent with the XRD and FTIR data. However, the residual solid was darker than the original Pb-jarosite, possessing a slightly higher chroma (10YR 7/8), and the post-dissolution grains exhibit selective dissolution pitting that appeared to follow the crystal habit (Fig. 8).

The molar ratios of the solid remaining after Pb-As-jarosite dissolution, calculated assuming SO_4^{2-} has a stoichiometric value of 1.69, were 0.430-0.433 for Pb, 3.129-3.135 for Fe, and 0.157-0.160 for AsO_4^{3-}. As for Pb-jarosite, the X-ray diffractograms and FTIR spectra did not indicate the presence of any new compound following dissolution of Pb-As-jarosite at pH 2 (compare Figs. 2a, 2b and 4a, 4b). However, the residual solid was slightly darker in colour (10YR 7.5/8) than the original material, and showed extensive internal dissolution pitting that resembled smooth tubular or spherical voids (Fig. 9). A very finely distributed, 1-5 nm diameter secondary compound covers all the Pb-As-jarosite grains (Fig. 9).

3.3. Dissolution at pH 8

3.3.1. Solution Composition

Concentrations of Pb and Fe in solution were very low throughout the pH 8 dissolution of Pb-jarosite (Fig. 10a, b). The Pb and SO_4^{2-} concentrations increased approximately linearly, while Fe reached a plateau near 0.0004 mmol L^{-1} (Fig. 10a, b; Table 1). The experiments were terminated at 2250 h, as steady state conditions were not observed. The pH decreased from 8.00 at the start of the experiment to 3.44-3.54 at the termination (Fig. 11; Table 1). The molar ratios of ions in solution, calculated assuming SO_4^{2-} has a stoichiometric value of 2, were 0.110-0.112 for Pb and 0.0063-0.0067 for Fe.

The SO_4^{2-} profile for the pH 8 dissolution of Pb-As-jarosite is sigmoidal and broadly resembles that for the pH 2 dissolution (compare Figs. 12a and 7a). By contrast, the AsO_4^{3-} concentration profile is curved and concave to the *t* axis, with a plateau at approximately 250 h (Fig. 12a). All but one of the Pb concentrations were below the detection limit of 5 ppb (Fig. 12a, b). Dissolved Fe concentration reaches a minimum near 250 h, rising slowly afterwards in a roughly linear fashion (Fig. 12a, b). The Pb-As-jarosite dissolution experiments were terminated at 2250 h as steady state conditions were not observed for SO_4^{2-}, Pb or Fe. The final pH of the Pb-As-jarosite suspensions, varying from 4.58 to 4.78, was somewhat less acidic than that for Pb-jarosite (Table

1). Molar ratios of the aqueous ions, calculated with respect to SO_4^{2-} (1.69), were 0.0097-0.0158 for Fe, and 0.175-0.190 for AsO_4^{3-} (Table 1). The final molar ratio for Pb was 0.0078, based on the single measurement that was above the detection limit. Because steady state was not achieved, we did not calculate equilibrium aqueous activites or saturation indices for the Pb- and Pb-As-jarosite dissolution experiments.

3.3.2. Residual Solids

Concentrations and molar ratios of Pb, Fe and SO_4^{2-} in the solids remaining after Pb-jarosite dissolution at pH 8 are summarised in Table 4. The Pb ratio in the residual solids varied from 0.178 – 0.183, and the Fe ratio from 3.639 – 3.673. XRD and FTIR analyses indicate that the principal constituent of the residue is Pb-jarosite (compare Figs. 1a, 1c and 3a, 3c), while the absence of unidentified peaks or bands suggests that no new compounds were present. Photomicrographs of the solids, however, show that there is a globular secondary compound, of 5 to 20 nm diameter, coating the grains (Fig. 13). This morphology is similar to that of ferrihydrite, which is described as having a spherical habit (Bigham, 1994). In contrast to the pH 2 Pb-jarosite dissolution experiments (Fig. 8), there is no evidence of selective dissolution along crystal faces. The residual solid is darker and redder than the original Pb-jarosite, reflected in the redder hue of the former (7.5 YR 4.5/7). This colour is similar to that of ferrihydrite found in ARD/AMD environments (5YR to 7.5YR; Bigham, 1994).

The Pb ratio in the Pb-As-jarosite residual solids varied from 0.412 – 0.415, with the Fe ratio varying from 3.396 – 3.412 and the AsO_4^{3-} ratio from 0.267 – 0.270 (Table 4). Additional bands and peaks were absent in the FTIR spectra and XRD patterns, indicating that no new compounds were present. The SEM data, however, suggest that poorly ordered secondary precipitates, 1-5 nm in diameter, are distributed across the grains. In contrast to the pH 2 Pb-As-jarosite dissolution, there is no evidence for surface pitting following dissolution at pH 8 (compare Figs. 9 and 14). The residual solid has a Munsell colour of 10YR 6.5/8, somewhat darker than the

unaltered Pb-As-jarosite. This colour, like that of the residual solid for Pb-jarosite, is not unlike that reported for ferrihydrite (Bigham, 1994).

4. DISCUSSION

4.1. Pb-jarosite

4.1.1. Dissolution at pH 2

The Pb, Fe, and SO_4^{2-} concentration profiles (Fig. 6) show a rapid initial release of constituent ions to solution followed by a decreasing rate of dissolution and eventually, quasi-steady state. The pH 2 Pb-jarosite dissolution reached steady-state more rapidly than a similar pH 2 dissolution of end-member K-jarosite (i.e., 1500 h compared to 3000 h; Smith *et al*., 2005). The main structural difference between the Pb-jarosite and K-jarosite is the A-site cation (i.e., Pb(II) versus K^+). The absence of an 11 Å (003) reflection in the Pb-jarosite XRD pattern (Fig. 1a) indicates that the Pb(II) ions and vacancies are not regularly ordered in the A-site. The strain imposed by Pb(II) incorporation in the A-site suggests that the Pb-jarosite structure is less stable than the K-jarosite structure, and may explain the reduced dissolution time and increased rate of dissolution during the first 500 h for Pb-jarosite (Fig. 6) compared to K-jarosite, even though both have similar specific surface areas (Smith *et al*., 2005).

The molar ratios of Pb and Fe in the residual solid are considerably higher than those in the unaltered Pb-jarosite, indicating that the residue is depleted in SO_4^{2-} relative to the original material (Table 4). The Pb aqueous molar ratios are slightly lower than that for the synthetic Pb-jarosite. Similarly, the Fe aqueous molar ratios are somewhat lower than those for the solid (Table 1). Thus, all the molar ratios reveal varying degrees of incongruent dissolution of Pb-jarosite at pH 2.

The pH 2 dissolution of Pb-jarosite is described as incongruent because of the non-stoichiometric dissolution of the parent solid, which can be described as follows:

$$(H_3O)_{0.74}Pb_{0.13}Fe_{2.92}(SO_4)_2(OH)_{5.76} + H^+_{(aq)} \rightarrow xPb^{2+}_{(aq)} + yFe^{3+}_{(aq)} + zSO^{3-}_{4(aq)} \quad (1)$$

Although the selective surface dissolution of the Pb-jarosite crystals suggests they may be compositionally zoned (Fig. 8), we explain it by the preferential removal of SO_4^{2-} groups closest to the mineral surface (cf. Gasharova *et al*., 2005; Smith *et al*., 2005). If reaction (1) were stoichiometrically balanced, then the IAP would be expressed as follows:

$$(H_3O)_{0.74}Pb_{0.13}Fe_{2.92}(SO_4)_2(OH)_{5.76} + 5.02H^+_{(aq)} \rightarrow$$

$$0.13Pb^{2+}_{(aq)} + 2.92Fe^{3+}_{(aq)} + 2SO^{3-}_{4(aq)} + 6.5H_2O_{(l)} \qquad (2)$$

$$\log IAP = 0.13\log\{Pb^{2+}\} + 2.92\log\{Fe^{3+}\} + 2\log\{SO_4^{2-}\} + 6.5\log\{H_2O\} + 5.02pH \qquad (3)$$

Although the speciation modelling and calculated saturation indices predict the stability of hematite and goethite and the dissolution of anglesite in our experimental system (Table 3), these calculations should be interpreted with caution. Anglesite, rather than Pb-jarosite, is the compound predicted to dissolve simply because the GWB thermodynamic database lacks data for Pb-jarosites. For this reason, the calculated saturation indices for hematite and goethite are probably incorrect, although it is likely that goethite will eventually precipitate as a result of the pH 2 dissolution of Pb-jarosite, as was observed experimentally for K-jarosite (Smith *et al*., 2005). Furthermore, as we cannot prove with our current data that thermodynamic equilibrium has been achieved, the GWB modelling provides only a qualitative description of the system. However, the lack of secondary precipitates and the maintenance of pH near 2 throughout the 2250 h experiment suggests that, as in many natural mine waste systems (cf., Dold and Fontboti, 2001), the dissolution of the Pb-jarosite in our model system may be approaching equilibrium, indicating that this solid likely governs the activity of free ions in solution.

4.1.2. Dissolution at pH 8

The pH 8 dissolution of Pb-jarosite is an incongruent reaction as indicated by the precipitation of a poorly crystalline $Fe(OH)_3$ secondary compound and the non-stoichiometric dissolution of Pb and SO_4^{2-} (Tables 1, 4). The concentrations of dissolved Pb and SO_4^{2-} greatly exceed those of Fe (Table 1), and the range of Pb aqueous molar ratios (Table 1) indicate that aqueous SO_4^{2-} is in slight excess

relative to Pb. This incongruency may arise from the relatively low occupancy of Pb in the A-site, thus permitting proportionally more SO_4^{2-} than Pb to be released during dissolution. The higher molar ratio of Pb in the residual solids (Table 4), compared to that for the original Pb-jarosite (i.e., 0.13), is more difficult to interpret, as the former represents the aggregate molar ratio of both the residual Pb-jarosite and the secondary compound. Despite this shortcoming, these ratios suggest that either more SO_4^{2-} than Pb is dissolved from the original Pb-jarosite, and / or that relatively more Pb than SO_4^{2-} is adsorbed to the $Fe(OH)_3$. The linear increase in aqueous Pb with time (Fig. 10) suggests, however, that there is little or no re-sorption of Pb to the $Fe(OH)_3$ by the end of the experiment. The slight decrease in aqueous Pb concentration near the beginning of the experiment (at $t \approx 100$ h, where pH = 4.58-4.82; Fig. 11) suggests that Pb may have sorbed to newly formed Fe hydroxide at this point, as Pb is known to sorb to Fe hydroxides such as ferrihydrite to form ternary surface complexes such as $\equiv FeOHPbSO_4$ (Webster *et al.*, 1998; Swedlund and Webster, 2001; Swedlund *et al.*, 2003). By the end of our experiment, the sorbed Pb was probably released to solution as the pH decreased to 3.44-3.56 (Fig. 11). For the final experimental conditions, the reaction is as follows:

$$(H_3O)_{0.74}Pb_{0.13}Fe_{2.92}(SO_4)_2(OH)_{5.76} + OH^-_{(aq)} \rightarrow xPb^{2+}_{(aq)} + yFe(OH)_{3(gel)} + zSO^{3-}_{4(aq)} \quad (4)$$

The reason for the pH increase at the beginning of the experiment (Fig. 11) is unclear, but it may reflect experimental error (with either the first reading being anomalously low or the second anomalously high). In any case, there are enough readings after the first two to confirm the downward trend in pH discussed above.

4.2. Pb-As-jarosite

4.2.1. Dissolution at pH 2

The aqueous Pb and SO_4^{2-} concentration profiles for the pH 2 Pb-As-jarosite dissolution experiment contrast sharply with those for Pb-jarosite dissolution. During the first 300 h of Pb-As-jarosite dissolution, both Pb and SO_4^{2-} aqueous concentrations decreased sharply (Fig. 7), after which Pb

concentration stabilized and SO_4^{2-} concentration increased in a roughly linear fashion. Throughout the dissolution, the aqueous Pb concentration was extremely low, with similarly low aqueous Pb molar ratios (Table 1). The molar ratio of Pb in the residual solid (Table 4) is greater than that for synthetic Pb-As-jarosite (i.e., 0.32). These data give evidence for the precipitation of a Pb-rich secondary compound, whose formation is most apparent near 300 h. Given the Pb and SO_4^{2-} concentration data presented here, and previous evidence from the synthesis of Pb-bearing jarosites (Dutrizac *et al*., 1980), it is likely that this new compound is poorly crystalline $PbSO_4$. Following removal of Pb during precipitation of $PbSO_4$, the rise in SO_4^{2-} concentration after 300 h is likely due to continued dissolution of the parent solid and subsequent formation of $PbSO_4$, although, because SO_4^{2-} is released in greater amounts than Pb, not all of the dissolved SO_4^{2-} is removed from solution through precipitation of $PbSO_4$.

The Fe and AsO_4^{3-} aqueous concentration profiles (Fig. 7a) plateau at approximately 250-300 h, when $PbSO_4$ precipitation is most evident. The aqueous molar ratios of Fe and AsO_4^{3-} (Table 1), and residual solid AsO_4^{3-} molar ratios (Table 4), which are nearly one-half of the synthetic ratio (i.e., 0.31), suggest that aqueous Fe and AsO_4^{3-} are in significant excess, compared to aqueous SO_4^{2-}. Even though the aqueous Fe molar ratio is approximately three times higher than that of the synthetic solid, the Fe molar ratio for the residual solid is slightly greater than that of the synthetic Pb-As-jarosite. The reason for this apparent contradiction is that the residual Pb-As-jarosite is highly SO_4^{2-} deficient, due primarily to the formation of the $PbSO_4$ secondary compound. If this compound had not formed during the early part of the dissolution, one may expect the aqueous concentrations of SO_4^{2-} and AsO_4^{3-} to have been in excess, relative to Pb and Fe. At the end of the experiment, however, aqueous Fe and AsO_4^{3-} were in excess compared to Pb and SO_4^{2-}. Moreover, AsO_4^{3-} was in excess relative to Fe, as shown by the range in aqueous Fe molar ratios (Table 1). These data are consistent with the incongruent dissolution of Pb-As-jarosite at pH 2. The reaction can be described as follows:

$$(H_3O)_{0.68}Pb_{0.32}Fe_{2.86}(SO_4)_{1.69}(AsO_4)_{0.31}(OH)_{5.59} + H^+_{(aq)} \rightarrow$$

$$xPbSO_{4(gel)} + yFe^{3+}_{(aq)} + zSO^{2-}_{4(aq)} + z' AsO^{3-}_{4(aq)} \quad (5)$$

4.2.2. Dissolution at pH 8

The extremely low aqueous Pb concentration at c. 28 h, coupled with a Pb molar ratio that is higher in the residual solid than the original Pb-As-jarosite, indicate that a Pb-rich secondary compound, probably $PbSO_4$, formed as a result of the dissolution. Formation of $PbSO_4$ would also explain the concentration profile of SO_4^{2-}, which is markedly different from those of Pb-jarosite (compare Figs. 10a and 12a) and end-member K-jarosite (Smith *et al.*, 2005), but is similar to that of the pH 2 dissolution of Pb-As-jarosite (Fig. 7a), in which $PbSO_4$ is also thought to form. During the first 1000 h of dissolution, SO_4^{2-} concentrations remained low due to precipitation of $PbSO_4$. Once Pb was largely removed from solution, SO_4^{2-}, released in greater amounts than Pb from Pb-As-jarosite, continued to increase, reaching a plateau near the termination of dissolution. The $PbSO_4$ is likely poorly crystalline, as crystalline $PbSO_4$ (anglesite) has a well-defined XRD pattern that was not observed in the residual solids. Moreover, anglesite yields a weak but distinctive band at 967 cm^{-1} in its FTIR spectrum, which was also not seen in the residual solids.

The aqueous Fe molar ratios (Table 1) and the residual solid Fe molar ratios (Table 4) indicate that an Fe-rich secondary compound is present in the residual solids. This Fe-rich compound is similar to the poorly crystalline $Fe(OH)_3$ observed following the pH 8 Pb-jarosite dissolution. The low AsO_4^{3-} aqueous molar ratios (Table 1) indicate a net deficiency of AsO_4^{3-} in solution. The residual solid AsO_4^{3-} ratios are also low, due to the probable precipitation of $PbSO_4$. These data suggest that a proportion of the aqueous AsO_4^{3-} has adsorbed to either or both of the secondary compounds. Many studies have demonstrated the feasibility of AsO_4^{3-} sorption to ferrihydrite (e.g., Raven *et al.*, 1998; Jain *et al.*, 1999; Richmond *et al.*, 2004) via the formation of inner-sphere bidentate binuclear corner and edge-sharing complexes (Sherman and Randall, 2003).

The pH 8 dissolution of Pb-As-jarosite can be described as follows:

$$(H_3O)_{0.68} Pb_{0.32} Fe_{2.86} (SO_4)_{1.69} (AsO_4)_{0.31} (OH)_{5.59} + OH^-_{(aq)} \rightarrow$$

$$xPbSO_{4(gel)} + yFe(OH)_{3(gel)} + zSO^{2-}_{4(aq)} + z' AsO^{3-}_{4(aq)} \quad (6)$$

This reaction is incongruent, as revealed by the presence of secondary compounds and the non-ideal dissolution of the parent solid.

4.3. Comparison of Pb-jarosite and Pb-As-jarosite Dissolutions, and Environmental Implications

The experimental data show that the pH 2 and 8 dissolutions of Pb- and Pb-As-jarosite are incongruent. Selective dissolution of the A-sites (containing Pb(II)) and T-sites (containing SO_4^{2-} and AsO_4^{3-}), results in higher concentrations of these ions in solution relative to Fe, which is located deep within the T-O-T structure in the original solid. Similar selective dissolution has also been documented for end-member K-jarosite (Becker and Gasharova, 2001; Gasharova *et al*. 2005; Smith *et al*., 2005). The selective dissolution of the A- and T-sites in Pb- and Pb-As-jarosite, reported here for the first time, has important implications for the geochemical pathways of Pb and As in the natural environment.

Poorly crystalline $PbSO_4$ is believed to form during the pH 2 and 8 dissolutions of Pb-As-jarosite, but not during the dissolution of Pb-jarosite. These two minerals differ by their Pb contents, and by the partial incorporation of AsO_4^{3-} at the T-site in the Pb-As-jarosite. It is hypothesized that this anion, in either or both the residual solid and solution, is shifting the thermodynamic equilibria of the system to favour $PbSO_4$ precipitation. Alternatively, greater amounts of selective dissolution of Pb from the Pb-As-jarosite relative to the Pb-jarosite (which contains less Pb than the Pb-As-jarosite) result in the saturation and precipitation of $PbSO_4$ as a result of dissolution of the former. The removal of aqueous Pb(II) by formation of $PbSO_4$ during Pb-As-jarosite dissolution has important implications for natural systems, as such precipitation reduces Pb(II) bioavailability.

During the pH 8 dissolutions of Pb- and Pb-As-jarosite, poorly crystalline $Fe(OH)_3$ precipitated, thus differing from similar pH 8 dissolutions of K-jarosite, in which secondary

goethite formed (Smith *et al.*, 2005). Precipitation of poorly crystalline $Fe(OH)_3$ following Pb- and Pb-As-jarosite dissolutions may have inhibited subsequent dissolution to such a degree that the concentration of Fe in solution was insufficient to form goethite directly. Over a longer period, however, it is highly probable that the poorly ordered $Fe(OH)_3$ will slowly crystallize into the more stable goethite (Bigham, 1994).

During the pH 2 dissolution of Pb- and Pb-As-jarosite approximately 20-25% of the original solid dissolved, with the amount of Pb-As-jarosite dissolved being slightly less due to the formation of $PbSO_4$, which may have inhibited the release of ions migrating from the dissolving solids into solution. Despite this hindrance, considerable amounts of AsO_4^{3-} are released to solution during the pH 2 dissolution of Pb-As-jarosite (Table 5). During the pH 8 dissolutions, approximately 10-15% of the original solids dissolved. In this case, the secondary $Fe(OH)_3$ may have acted as a dissolution inhibitor, thus limiting Pb-As-jarosite dissolution, in which less than 1% of the mobilised Pb remained in solution (Table 5). The low amounts of Pb and AsO_4^{3-} released to solution during the pH 8 dissolutions of Pb-As-jarosite, and to a lesser extent, Pb-jarosite may also be due to the sorption of these ions onto the surfaces of the secondary precipitates, although the amount of Pb sorption during the pH 8 Pb-jarosite dissolution appears to be small (Fig. 10b). Overall, therefore, the processes described in this paper are those of dissolution-precipitation rather than simply dissolution.

This study has shown that secondary $Fe(OH)_3$ forms when Pb- and Pb-As-jarosites dissolve in alkali environments, a phenomenon that has been predicted previously for plumbojarosite (Patino *et al.*, 1998). Although we found no evidence for the formation of other metastable compounds during the dissolutions, we sampled the residual solid only after several hundred hours had passed, and thus may have characterized only the stable end-product. The $Fe(OH)_3$ we observed may develop from the original, or slightly re-arranged, FeO_6 octahedra that remain after the preferential dissolution of Pb, SO_4^{2-} and AsO_4^{3-} or, alternatively, by precipitation of fully hydrated, dissolved

$Fe^{3+}_{(aq)}$ (cf., Table 2). The extremely low solubility of $Fe^{3+}_{(aq)}$ in oxic environments (< 10^{-18} M at pH 6; Schwertmann, 1991) will favour such precipitation.

CONCLUSIONS

The dissolutions of Pb- and Pb-As-jarosites at both pH 2 and 8 are incongruent, with selective dissolution of Pb, SO_4^{2-} and AsO_4^{3-} compared to Fe. As with end-member K-jarosite, this incongruency arises from the high stability of the FeO_6 octahedra within the T-O-T jarosite structure. Poorly crystalline $PbSO_4$ is inferred to form during the pH 2 and 8 dissolutions of Pb-As-jarosite, but not Pb-jarosite; this difference may be due to the partial incorporation of AsO_4^{3-} at the T-site in the former. The pH 2 dissolution of Pb-jarosite yields aqueous Pb, Fe and SO_4^{2-}, while that of Pb-As-jarosite yields Fe and SO_4^{2-}, AsO_4^{3-} and poorly crystalline $PbSO_4$. The pH 8 dissolutions of both Pb- and Pb-As-jarosite result in formation of poorly crystalline $Fe(OH)_3$ (possibly ferrihydrite), which sorbs aqueous AsO_4^{3-} during Pb-As-jarosite dissolution but appears not to sorb Pb during Pb-jarosite dissolution. The preliminary results of these complex dissolution reactions of Pb- and Pb-As-jarosites, presented here for the first time, shed important new light on the environmentally relevant geochemical pathways of Pb and As in ARD/AMD environments. Future work should examine the dissolution kinetics and products of a full range of Pb- and Pb-As-jarosite compositions, including the end-members plumbojarosite and beudantite, at different pH values, temperatures, aqueous phase mixing rates and suspension densities, carrying out full characterisation of the resultant products.

ACKNOWLEDGEMENTS

This work was funded through a UK Engineering and Physical Sciences Research Council (EPSRC) studentship award (number 309778) to A.M.L. Smith. We thank A.S. Wills for the GSAS refinement of the original synthetic jarosite, J. Wilson for assistance with thermodynamic modelling, C. Jones and A. Ball for help with SEM analysis and photography, G. Jones and V. Din

for assistance with geochemical analysis, and I. Wood, G. Cressey and C. Kirk for expert help with the XRD analysis. We also thank two anonymous referees and chief editor Prof. David Rickard, for many insightful comments and suggestions that substantially improved the manuscript.

REFERENCES

Alcobe X., Bassas J., Tarruella I., Roca A., Vinals J., 2001. Structural characterization of synthetic beudantite-type phase by Rietveld refinement. Epdic 7: European Power Diffraction, Pts 1 and 2 378-3, 671-676.

Alpers C.N., Rye R.O., Nordstrom D.K., Ball J.W., 1989. Solubility of jarosite solid solutions precipitated from acid mine waters, Iron Mountain, California., U.S.A. Sci. Géol. Bull. 42, 281-298.

Amrhein, C., Suarez, D.L., 1992. Some factors affecting the dissolution kinetics of anorthite at 25 degrees C. Geochim. Cosmochim. Acta 56, 1815-1826.

Baron, D., Palmer, C.D., 1996. Solubility of jarosite at 4-35ºC. Geochim. Cosmochim. Acta 60, 185-195.

Becker U., Gasharova B., 2001. AFM observations and simulations of jarosite growth at the molecular scale: probing the basis for the incorporation of foreign ions into jarosite as a storage mineral. Phys. Chem. Mineral. 28, 545-556.

Bethke C.M., 1996. Geochemical Reaction Modeling. Oxford University Press, New York.

Bigham J.M., 1994. Mineralogy of ochre deposits formed by sulphide oxidation. In: Jambor, J.L., Blowes, D.W. (Eds.), The Environmental Geochemistry of Sulfide Mine-Wastes, Mineralogical Association of Canada Short Course 22, pp. 103-132.

Bigham J. M., Nordstrom D. K. 2000. Iron and aluminium hydroxysulfates from acid sulphate waters. In: Alpers, C.N., Jambor, J.L., Nordstrom, D.K. (Eds.), Sulfate Minerals: Crystallography, Geochemistry, and Environmental Significance, Reviews in Mineralogy and Geochemistry 40, pp. 351-403.

Brophy G.P., Sheridan M.F., 1965. Sulfate studies IV: The jarosite-natrojarosite-hydronium jarosite solid solution series. Am. Miner. 50, 1595-1607.

Brunauer S., Emmett P.H., Teller E., 1938. Adsorption of gases in multimolecular layers. J. Am. Chem. Soc. 60, 309-319.

Crundwell F.K., Bryson A.W., 1992. The modelling of particular leaching reactors – the population balance approach. Hydrometallurgy 29, 275-295.

Dold, B., Fontboti, L., 2001. Element cycling and secondary mineralogy in porphyry copper tailings as a function of climate, primary mineralogy, and mineral processing. J. Geochem. Explor. 74, 3-55.

Drouet, C., Navrotsky, A., 2003. Synthesis, characterization, and thermochemistry of K-Na-H_3O jarosites. Geochim. Cosmochim. Acta 67, 2063-2076.

Dubinina V.N., Kornilovich I.A., 1959. Plumbojarosite in the oxidation zone of Pb-Zn ore deposits of Eastern Transbaikal. Zap. Vses. Mineral. Obshch. 88, 323-328.

Dutrizac J.E., 1983. Factors affecting alkali jarosite precipitation. Metall. Trans. B 14B, 531-539.

Dutrizac J.E., Chen T.T., 2003. Synthesis and properties of V3+ analogues of jarosite-group minerals. Canadian Mineral. 41, 479-488.

Dutrizac J.E., Kaiman S., 1976. Synthesis and properties of jarosite-type compounds. Can. Miner. 14, 151-158.

Dutrizac J.E., Dinardo O., Kaiman S., 1980. Factors affecting lead jarosite formation. Hydrometall. 5, 305-324.

Gasharova B., Göttlicher J., Becker U., 2005. Dissolution at the surface of jarosite: an in-situ AFM study. Chem. Geol. 215, 499-516.

Härtig C., Brand P., Bohmhammel K., 1984. Fe-Al-Isomorphie and Strukturwasser in Kristallen vom Jarosit-Alunit-Typ. Z. Anorg. Allg. Chem. 508, 159-164.

Hawthorne F.C., Krivovichev S.V., Burns, P.C., 2000. The crystal chemistry of sulphate minerals. In: Alpers, C.N., Jambor, J.L., Nordstrom, D.K. (Eds.), Sulfate Minerals: Crystallography,

Geochemistry, and Environmental Significance, Reviews in Mineralogy and Geochemistry 40, pp. 1-112.

Helgeson H.C., 1969. Thermodynamics of hydrothermal systems at elevated temperatures and pressures. Am. J. Sci. 267, 729-804.

Hendricks S.B., 1937. The crystal structure of alunite and the jarosites. Am. Miner. 22, 773-784.

Hochella M.F., Moore J.N., Golla A., Putnis A., 1999. A TEM study of samples from acid mine drainage systems: Metal-mineral association with implications for transport. Geochim. Cosmochim. Acta 63, 3395-3406.

Hudson-Edwards K.A., Schell C., Macklin M.G., 1999. Mineralogy and geochemistry of alluvium contaminated by metal mining in the Rio Tinto area, southwest Spain. Appl. Geochem. 14, 55-70.

Jain A., Raven K.P., and Loeppert R.H., 1999. Arsenite and arsenate adsorption of ferrihydrite: surface charge reduction and net OH- release stoichiometry. Env. Sci. Technol. 33, 1179-1184.

Jambor J.L. 1999. Nomenclature of the alunite supergroup. Can. Miner. 37, 1323-1341.

Kubisz J., 1964. A study of minerals in the alunite-jarosite group. Polska Akad. Nauk. Prace Geol. 22, 1-93.

Kubisz J., 1970. Studies on synthetic alkali-hydronium jarosites. I. Synthesis of jarosite and natrojarosite. Mineralogia Polonica 1, 47-57.

Larson A.C., Von Dreele R.B., 1998. Computer-simulation studies of perfect and defective surfaces in Cr_2O_3. J. Am. Ceramic Soc. 71, C389-C391.

Le Bail A., Duroy H., Fourquet J.L., 1988. Abinitio structure determination of $LiSBWO_6$ by X-ray powder diffraction. Materials Res. Bull. 23, 447-452.

Patino F., Viñals J., Roca A., Nunez C., 1994. Alkaline decomposition – cyanidation kinetics of argentian plumbojarosite in CaO media. Revista Soc. Quim. Mexico 42, 122-128.

Patino F., Arenas A., Rivera I., Cordoba D.A., Hernandez L., Salinas E., 1998. Decomposition of argentiferous plumbojarosite in CaO media. Revista Soc. Quim Mexico 42, 122-128.

Powers D.A., Rossman G.R., Schugar H.J., Gray H.B., 1975. Magnetic behaviour and infrared spectra of jarosite, basic iron sulphate and their chromate analogues. J. Sol. Stat. Chem. 13, 1-13.

Raven K.P., Jain A., Loeppert R.H., 1998. Arsenite and arsenate adsorption on ferrihydrite: kinetics, equilibrium, and adsorption envelopes. Env. Sci. Technol. 32, 344-349.

Richmond W.R., Loan M., Morton J., Parkinson G.M., 2004. Arsenic removal from aqueous solution via ferrihydrite crystallization control. Env. Sci. Technol. 38, 2368-2372.

Rickard, D., Sjvberg, E.L., 1983. Mixed kinetic control of calcite dissolution rates. Am. J. Sci. 283, 815-830.

Ripmeester J.A, Ratcliffe C.I., Dutrizac J.E., Jambor J.L., 1986. Hydronium in the alunite-jarosite group. Can. Miner. 22, 773-784.

Roca A., Viñals J., Arranz M., Calero J., 1999. Characterization and alkaline decomposition / cyanidation of beudantite-jarosite materials from Rio Tinto gossan ores. Can. Metall. Quart. 38, 93-103.

Rousel C., Neel C., Bril H., 2000. Minerals controlling arsenic and lead solubility in an abandoned gold mine tailings. Sci. Total Environ. 263, 209-219.

Schwertmann U., 1991. Solubility and dissolution of iron oxides. Plant and Soil 130, 1-25.

Serna C.J., Cortina C.P., Raymos J.V.G., 1986. Infrared and Raman-study of alunite jarosite compounds. Spectrachim. Acta 42, 729-734.

Sherman D.M., Randall S.R., 2003. Surface complexation of arsenic(V) to iron(II) (hydr)oxides: Structural mechanism from ab initio molecular geometries and EXAFS spectroscopy. Geochim. Cosmochim. Acta 67, 4223-4230.

Simons F.S., Mapes V.E., 1956. Geology and ore deposits of the Zimapán mining district, State of Hidalgo, Mexico. US Geol. Survey Prof. Paper 284.

Sjvberg, E.L., Rickard, D., 1983. The influence of experimental design on the rate of calcite dissolution. Geochim. Cosmochim. Acta 47, 2281-2285.

Smedley P.L., Kinniburgh D.G., 2002. A review of the sources, behaviour and distribution of arsenic in natural waters. Appl. Geochem. 17, 517-568.

Smith A.M.L., Hudson-Edwards K.A., Dubbin W.E., Wright K., 2005. Dissolution of jarosite [$KFe_3(SO_4)_2(OH)_6$] at pH 2 and 8: insights from batch experiments and computational modelling. Geochim. Cosmochim. Acta, in press.

Swedlund P.J, Webster J.G., 2001. Cu and Zn ternary surface complex formation with SO4 on ferrihydrite and schwertmannite. Appl. Geochem. 16, 503-511.

Swedlund P.J., Webster J.G., Miskelly G.M., 2003. The effect of SO_4 on the ferrihydrite adsorption of Co, Pb and Cd: ternary complexes and site heterogeneity. Appl. Geochem. 18, 1671-1689.

Vasilevskay G.B., 1970. Minerals in the oxidation zone of the Shamyrasi complex ore deposits. Nauch Trudy Tashkent Gosudarst Univ. 358, 131-134.

Vinals J., Roca A., Arranz M., 2003. Autoclave alkaline decomposition and cyanidation of jarosite-beudantite phases from Rio Tinto gossan ores. Can. Metall. Quart. 42, 29-40.

Webster J.G., Swedlund P.J., Webster K.S., 1998. Trace metal adsorption onto an acid mine drainage iron(III) oxyhydroxysulfate. Environ. Sci. Technol. 32, 1361-1368.

Wolery T., 1979. Calculation of equilibrium between aqueous solution and minerals: the EQ3/6 software package. Lawrence Livermore National Laboratory, UCRL-52658.

Wolery T., 1996. EQ3/6 Database. Lawrence Livermore National Laboratory, USA.

FIGURES

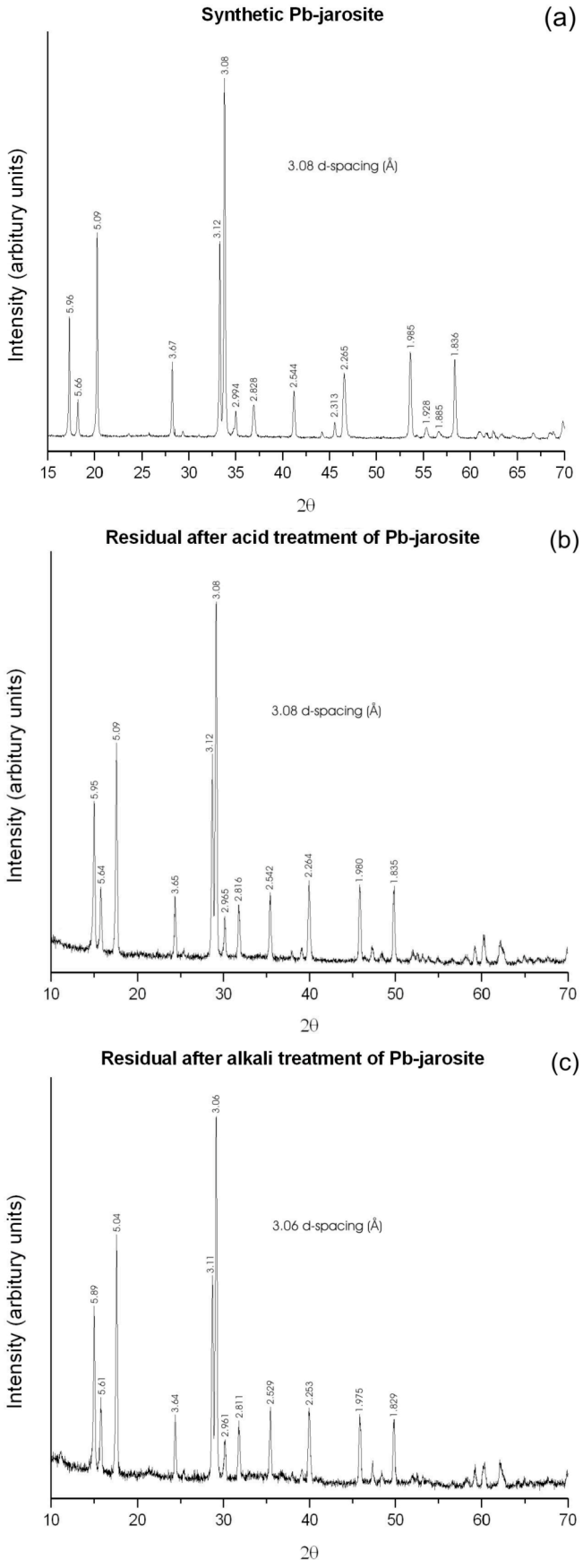
Synthetic Pb-jarosite
(a)
Intensity (arbitury units)
3.08 d-spacing (Å)
3.08
5.09
3.12
5.96
3.67
5.66
2.994
2.828
2.544
2.313
2.265
1.985
1.928
1.885
1.836
15 20 25 30 35 40 45 50 55 60 65 70
2θ
Residual after acid treatment of Pb-jarosite
(b)
Intensity (arbitury units)
3.08 d-spacing (Å)
3.08
5.09
3.12
5.95
5.64
3.65
2.965
2.816
2.542
2.264
1.980
1.835
10 20 30 40 50 60 70
2θ
Residual after alkali treatment of Pb-jarosite
(c)
Intensity (arbitury units)
3.06 d-spacing (Å)
3.06
5.04
3.11
5.89
5.61
3.64
2.961
2.811
2.529
2.253
1.975
1.829
10 20 30 40 50 60 70
2θ

Figure 1: Powder X-ray diffraction patterns for Pb-jarosite. (a) Synthetic Pb-jarosite (b) pH 2 dissolution residual solids, and (c) pH 8 dissolution solids. d-spacings are indicated for the strongest reflections.

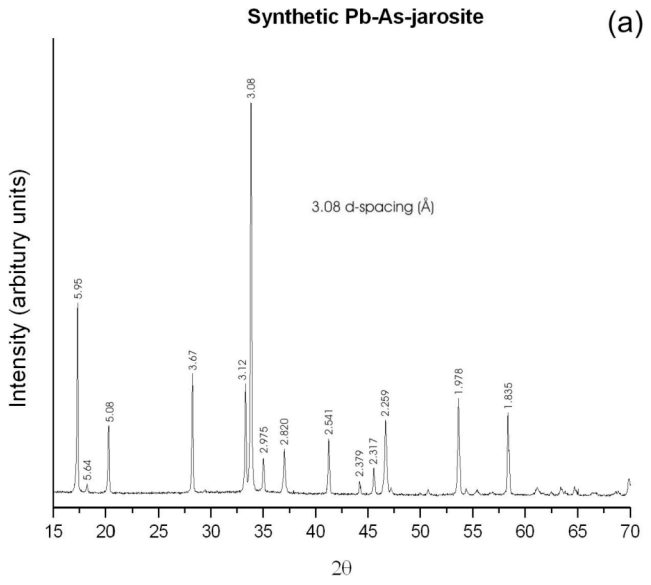
Synthetic Pb-As-jarosite
(a)
Intensity (arbitury units)
3.08 d-spacing (Å)
5.95
5.64
5.08
3.67
3.12
3.08
2.975
2.820
2.541
2.379
2.317
2.259
1.978
1.835
15 20 25 30 35 40 45 50 55 60 65 70
2θ

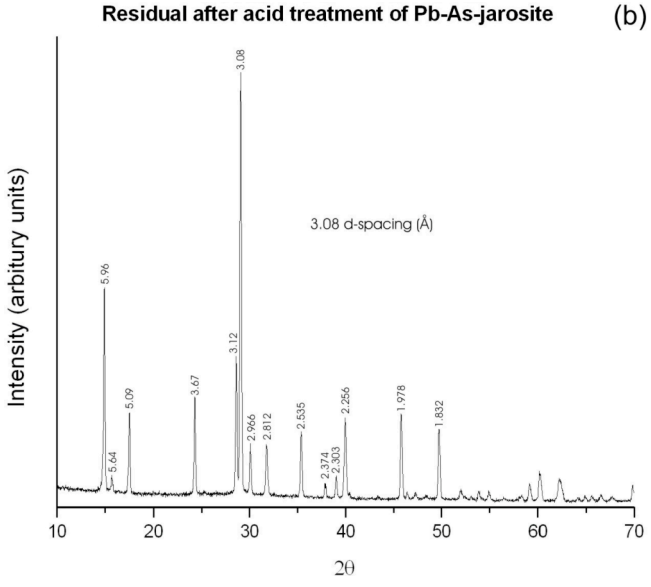
Residual after acid treatment of Pb-As-jarosite
(b)
Intensity (arbitury units)
3.08 d-spacing (Å)
5.96
5.64
5.09
3.67
3.12
3.08
2.966
2.812
2.535
2.374
2.303
2.256
1.978
1.832
10 20 30 40 50 60 70
2θ

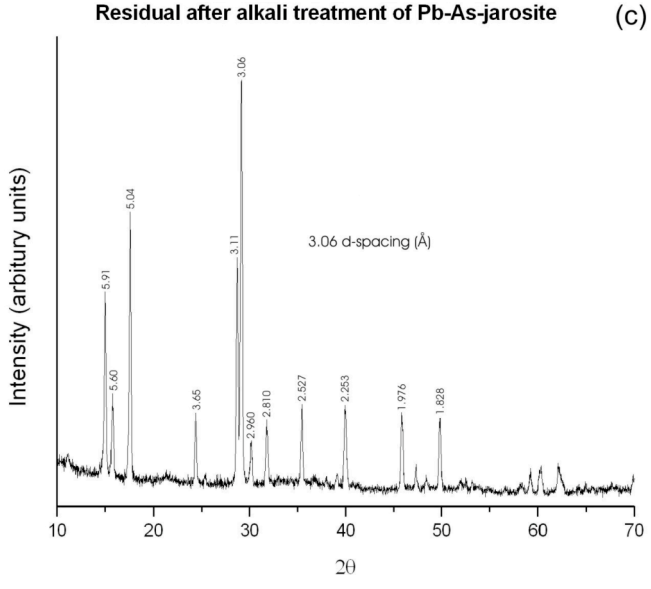
Residual after alkali treatment of Pb-As-jarosite
(c)
Intensity (arbitury units)
3.06 d-spacing (Å)
5.91
5.60
5.04
3.65
3.11
3.06
2.960
2.810
2.527
2.253
1.976
1.828
10 20 30 40 50 60 70
2θ

Figure 2: Powder X-ray diffraction patterns for Pb-As-jarosite. (a) Synthetic Pb-As-jarosite (b) pH 2 dissolution residual solids, and (c) pH 8 dissolution solids. d-spacings are indicated for the strongest reflections.

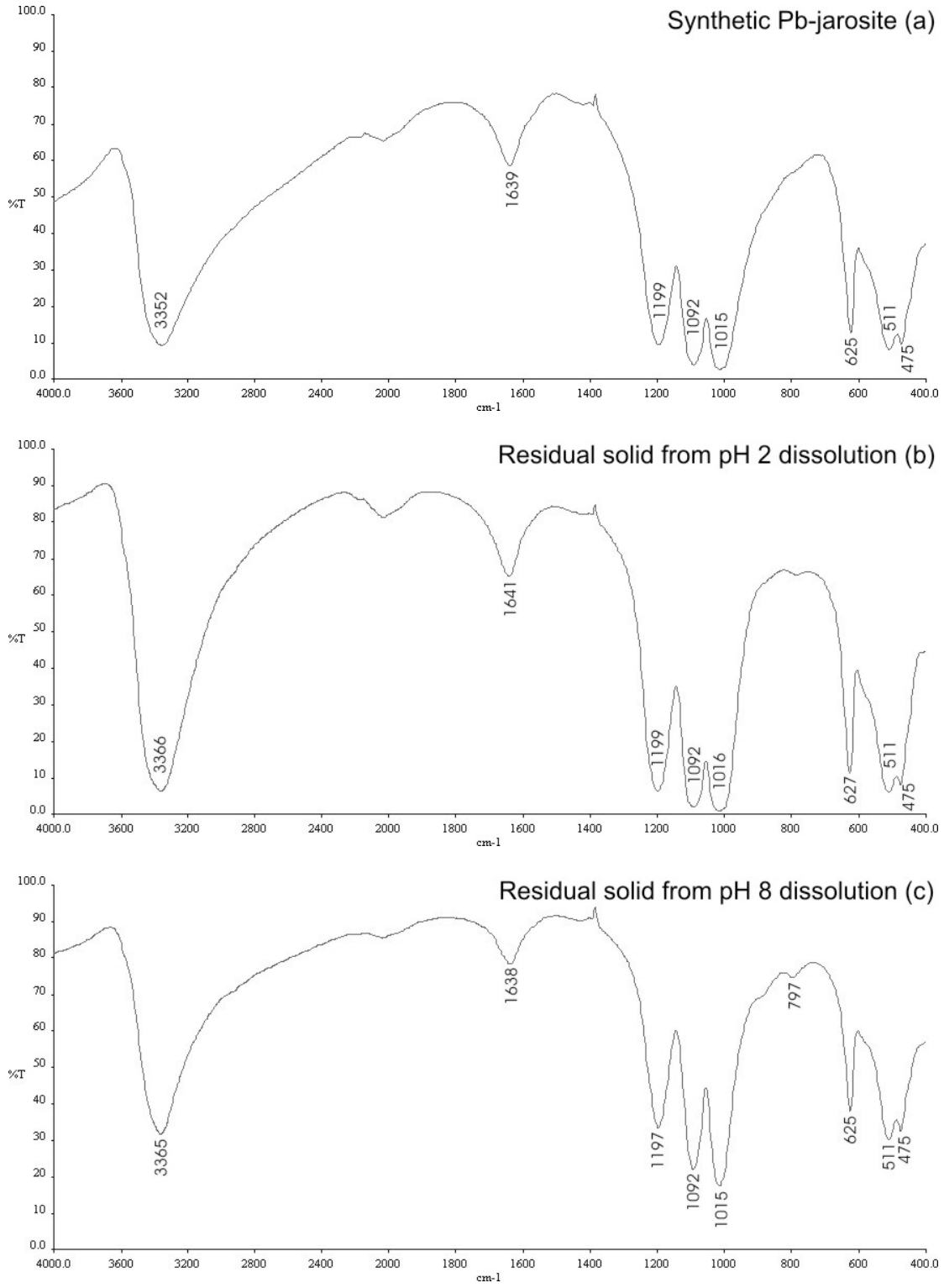

Figure 3. Fourier transform infrared (FTIR) spectra for Pb-jarosite. (a) Synthetic Pb-jarosite; (b) pH 2 dissolution residual solids; (c) pH 8 dissolution residual solids. The main vibrational bands in the spectra are marked.

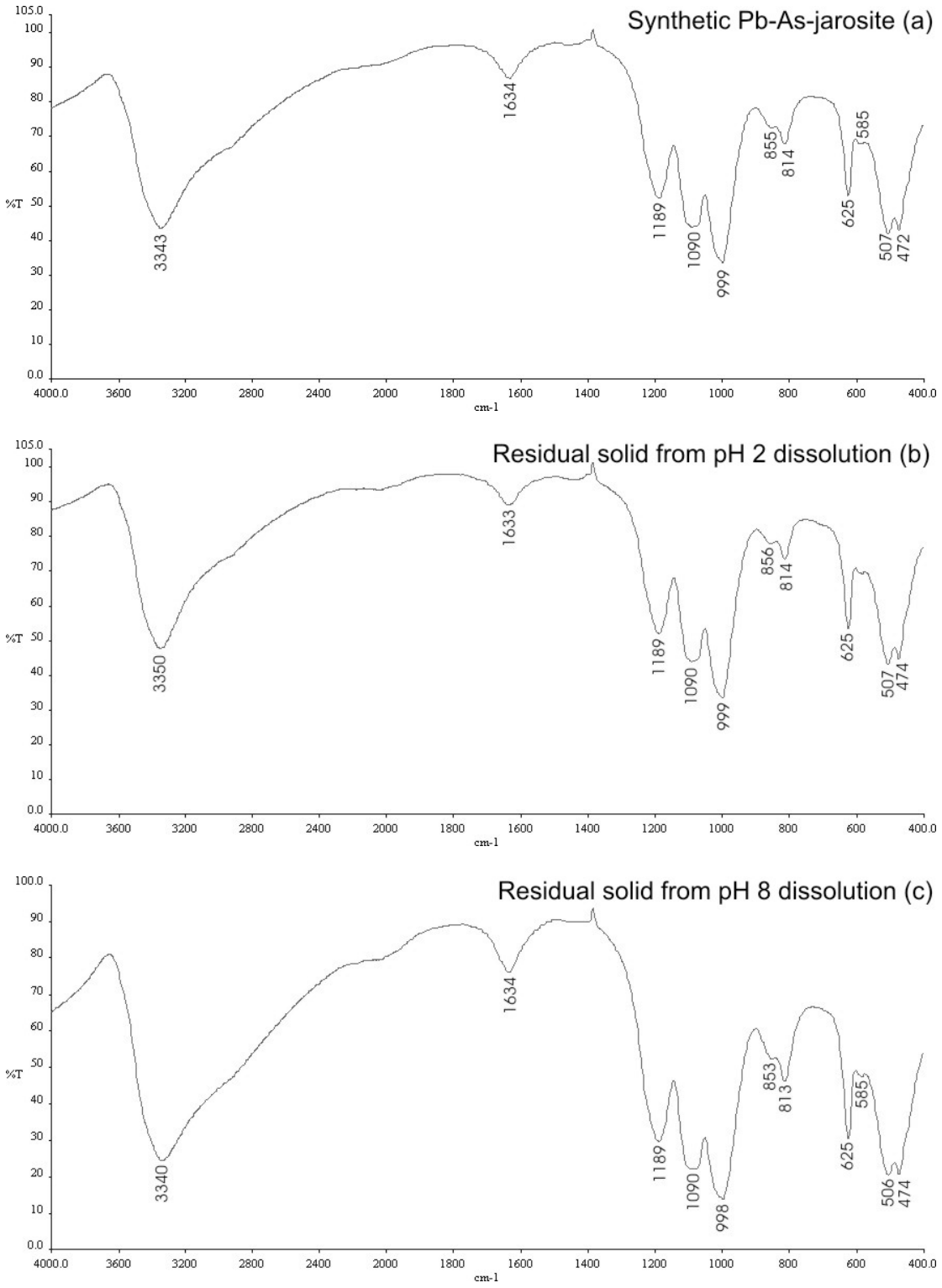

Figure 4. Fourier transform infrared (FTIR) spectra for Pb-As-jarosites. (a) Synthetic Pb-As-jarosite; (b) pH 2 dissolution residual solids; (c) pH 8 dissolution residual solids.

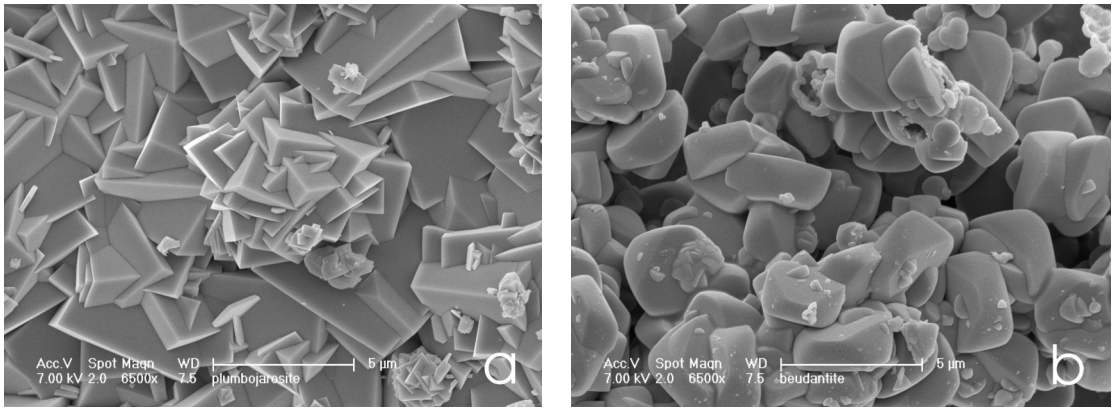

Figure 5. Scanning electron microscope (SEM) images of synthetic (a) Pb-jarosite and (b) Pb-As-jarosite. The scale bar on the micrographs is 5 µm.

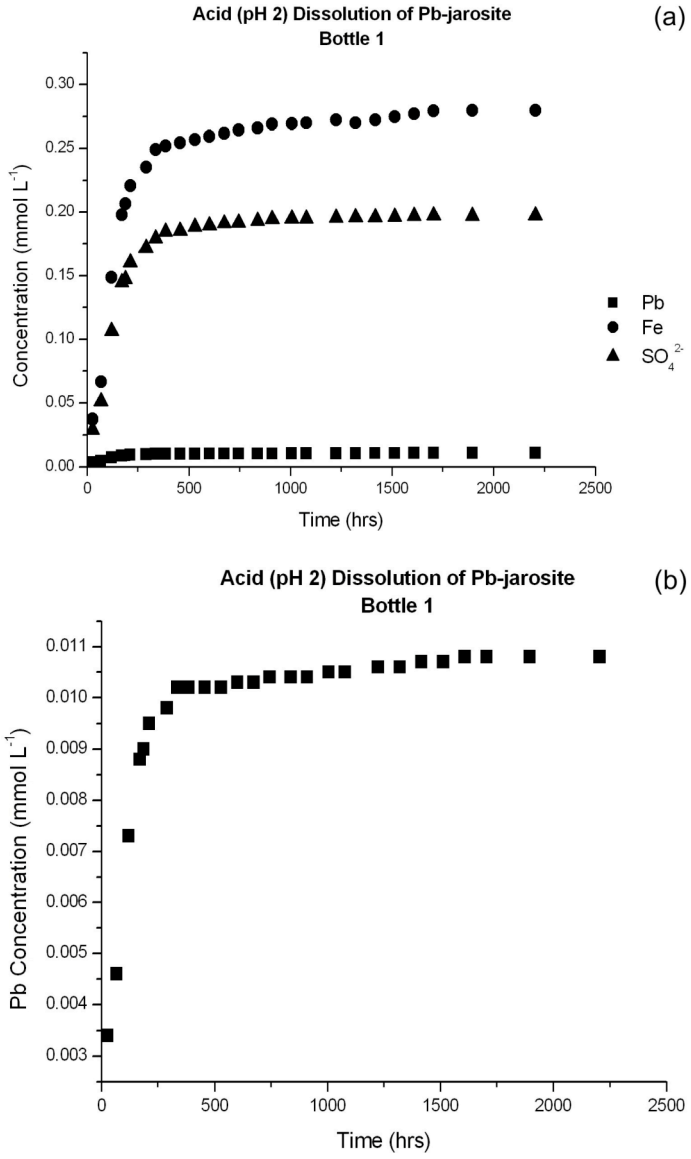

Figure 6 (a) Concentrations of Pb_{tot}, Fe_{tot} and $SO_4^{2-}{}_{tot}$ in solution for the pH 2 dissolution of Pb-jarosite plotted against time ($pH_{initial}$ = 2.00). (b) Concentrations of Pb_{tot} in solution re-plotted from (a) on a more appropriate scale.

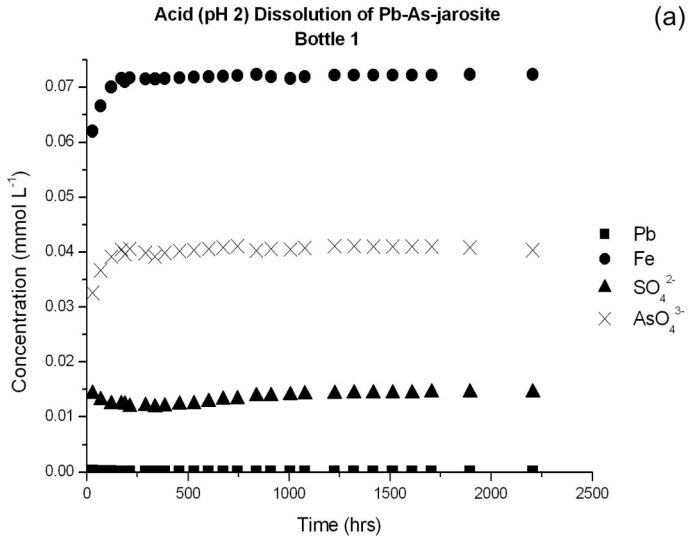
Acid (pH 2) Dissolution of Pb-As-jarosite
Bottle 1
(a)
Concentration (mmol L-1)
Time (hrs)
Pb
Fe
SO4 2-
AsO4 3-

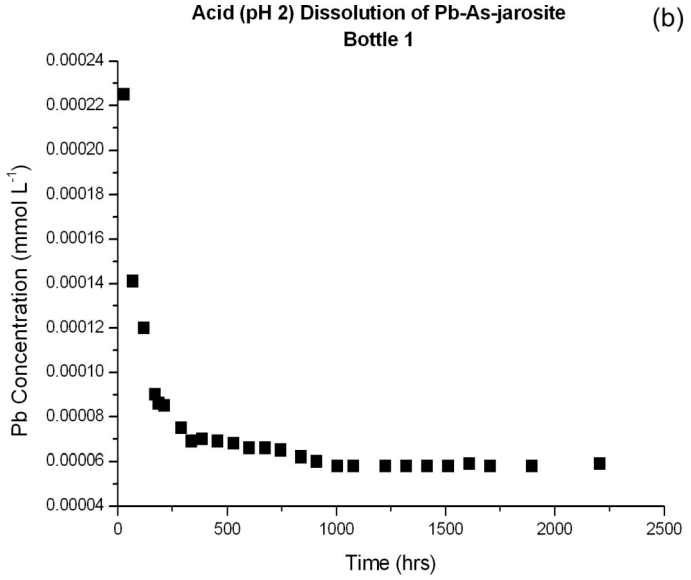
Acid (pH 2) Dissolution of Pb-As-jarosite
Bottle 1
(b)
Pb Concentration (mmol L-1)
Time (hrs)

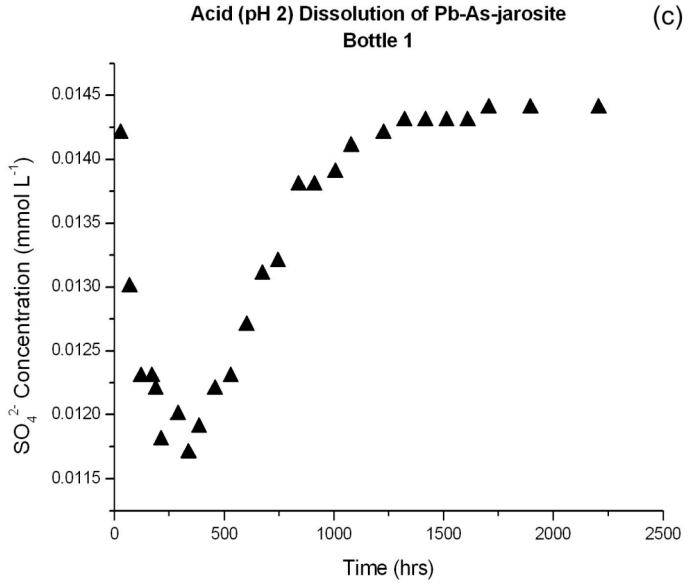
Acid (pH 2) Dissolution of Pb-As-jarosite
Bottle 1
(c)
SO4 2- Concentration (mmol L-1)
Time (hrs)

Figure 7. (a) Concentrations of Pb_{tot}, Fe_{tot}, $SO_4^{2-}{}_{tot}$ and $AsO_4^{3-}{}_{tot}$ in solution for the pH 2 dissolution of Pb-As-jarosite plotted against time ($pH_{initial}$ = 2.00); (b) Concentrations of Pb_{tot} in solution re-plotted from (a) on a more appropriate scale; (c) Concentrations of $SO_4^{2-}{}_{tot}$ in solution re-plotted from (a) on a more appropriate scale.

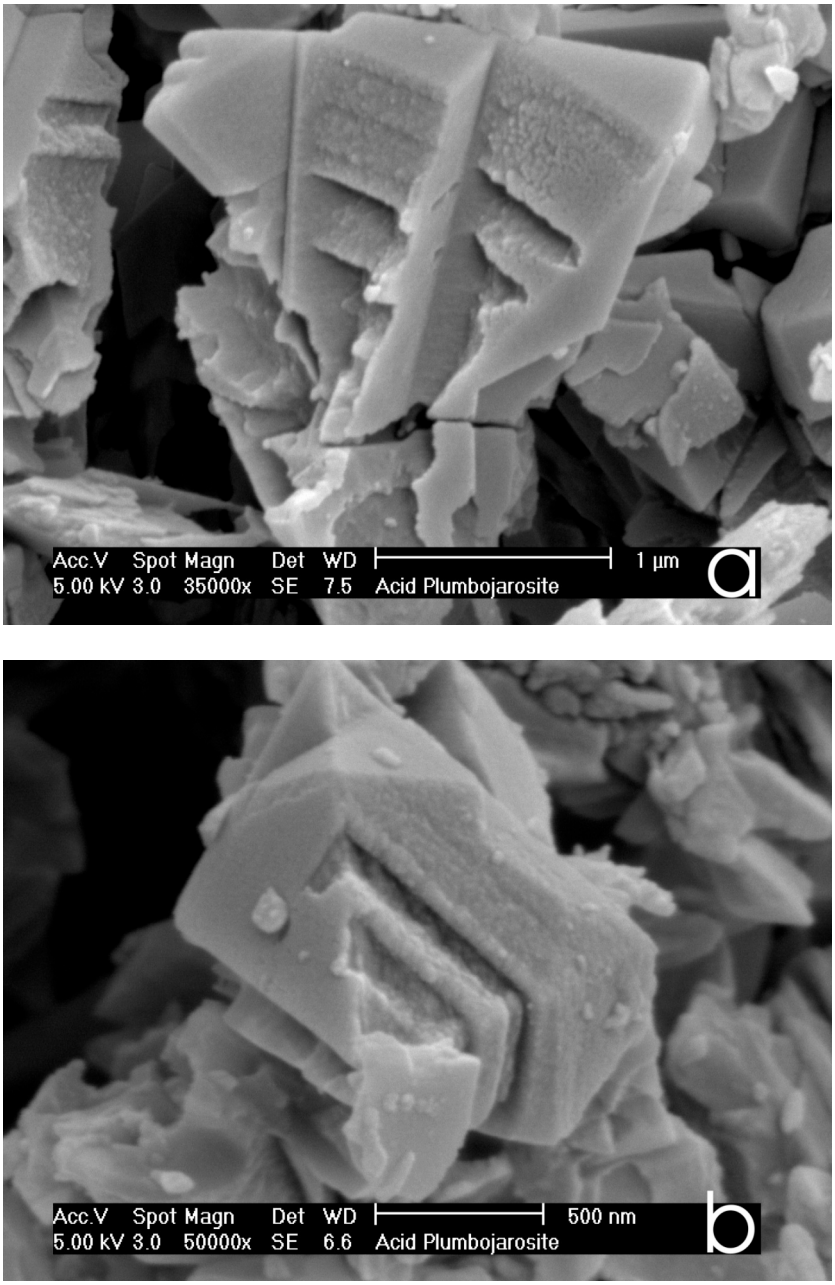

Figure 8. Scanning electron microscope (SEM) images of the residual solid from the pH 2 dissolution of Pb-jarosite. Image (a) highlights dissolution morphology common throughout the sample. Image (b) is a high-resolution micrograph of a single grain, showing selective dissolution at the surface. Operating conditions are indicated on each micrograph.

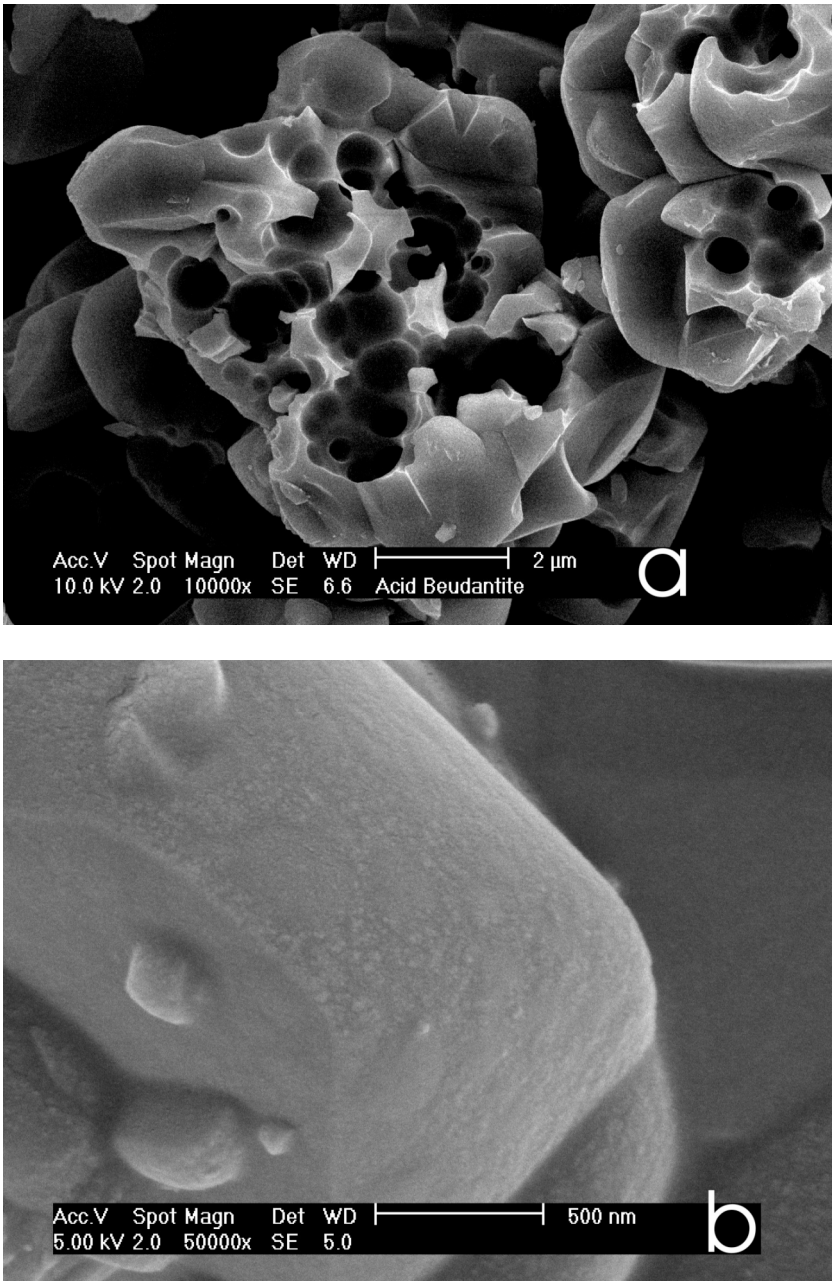

Figure 9. Scanning electron microscope (SEM) images of the residual solid from the pH 2 dissolution of Pb-As-jarosite. Image (a) is an overview showing extensive pitting of the surface. Image (b) is a high-resolution micrograph of a single grain, showing a very finely dispersed secondary phase, probably poorly crystalline $PbSO_4$, on the surface. Operating conditions indicated on each micrograph.

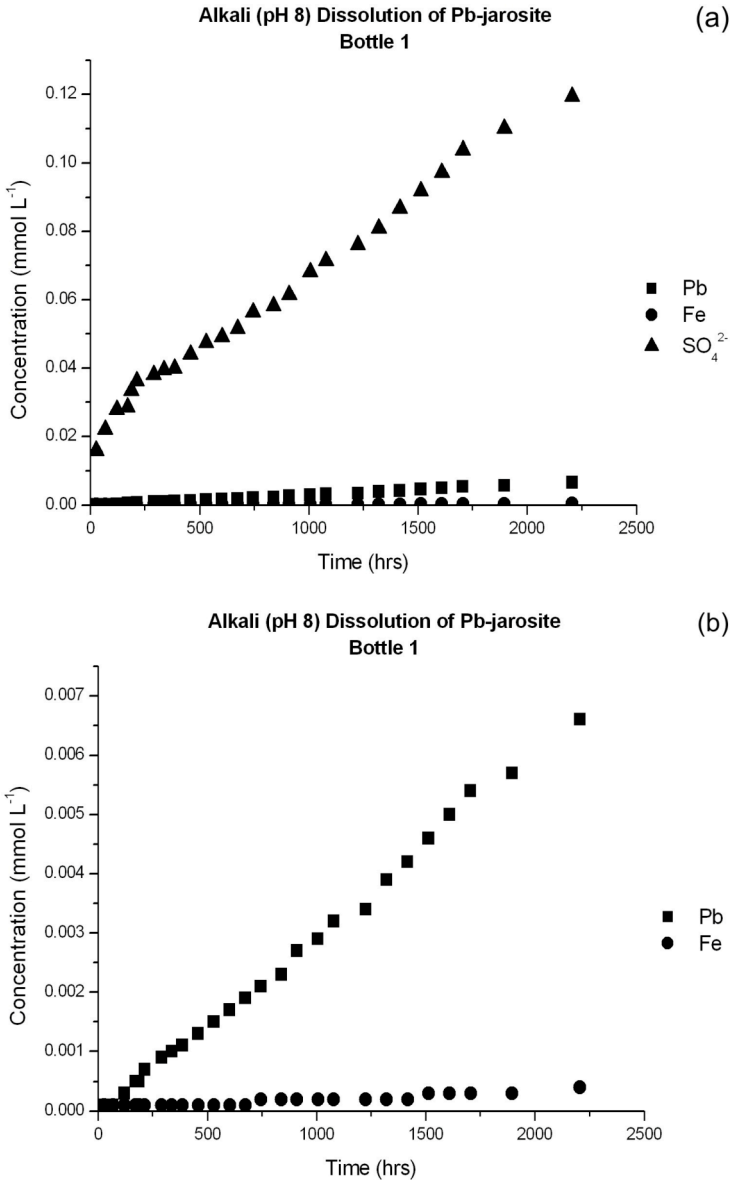

Figure 10. (a) Concentrations of Pb_{tot}, Fe_{tot} and $SO_4^{2-}{}_{tot}$ in solution for the pH 8 dissolution of Pb-jarosite plotted against time ($pH_{initial}$ = 8.00); (b) Concentrations of Pb_{tot} and Fe_{tot} in solution re-plotted from (a) on a more appropriate scale.

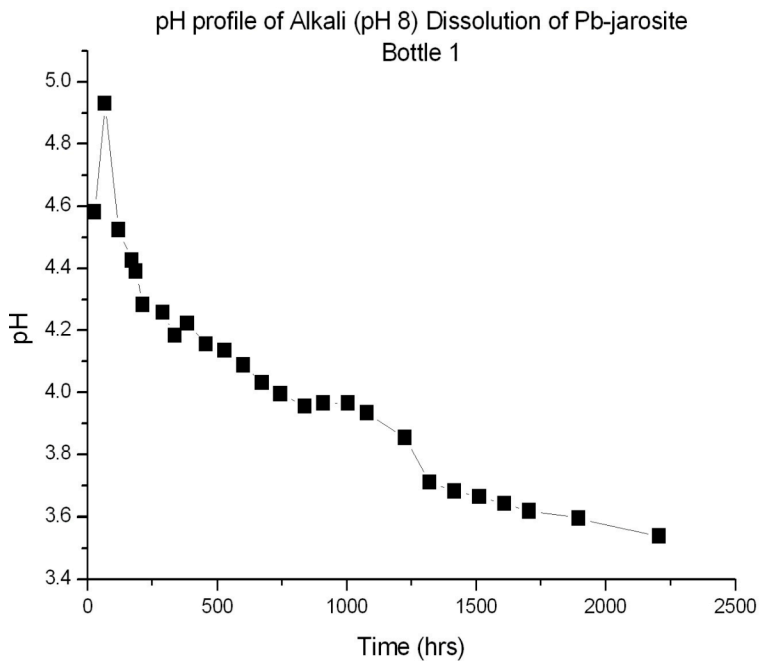

Figure 11. Plot of pH vs. time (h) for dissolution of Pb-jarosite ($pH_{initial}$ = 8.00).

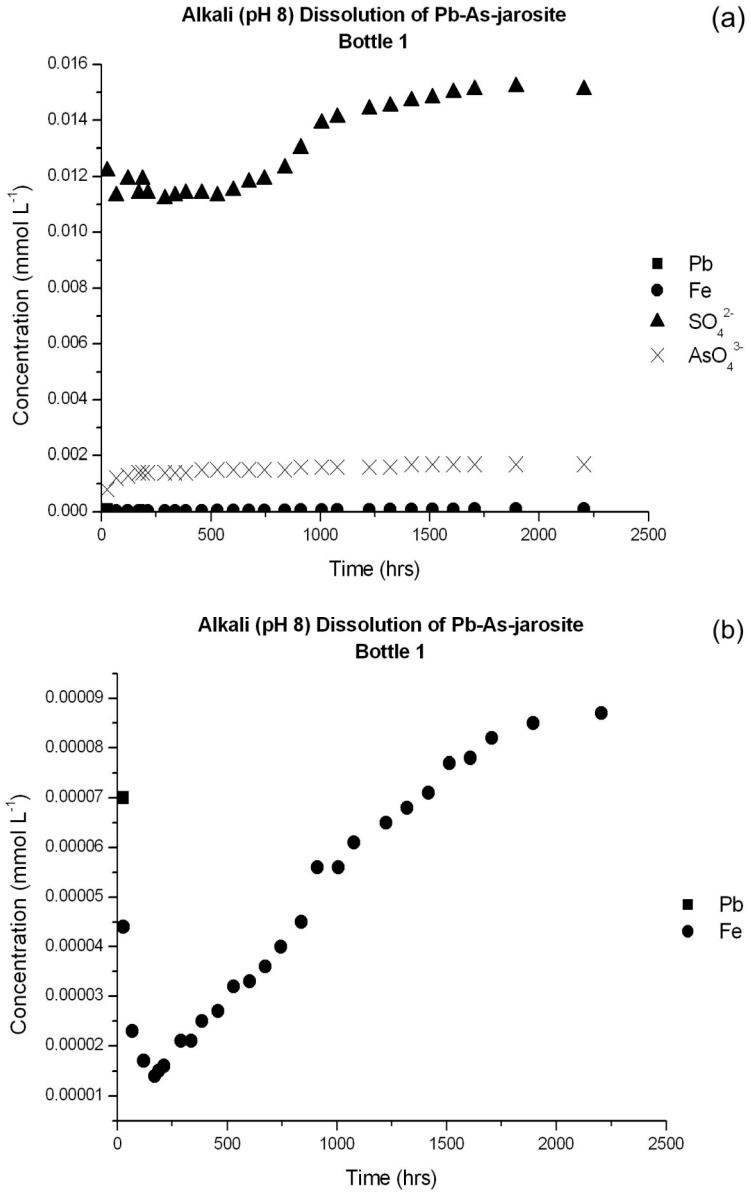

Figure 12. (a) Concentrations of Pb_{tot}, Fe_{tot}, $SO_4^{2-}{}_{tot}$ and $AsO_4^{3-}{}_{tot}$ in solution for the pH 8 dissolution of Pb-As-jarosite plotted against time ($pH_{initial}$ = 8.00); (b) Concentrations of Pb_{tot} and Fe_{tot} in solution re-plotted from (a) at a more appropriate scale.

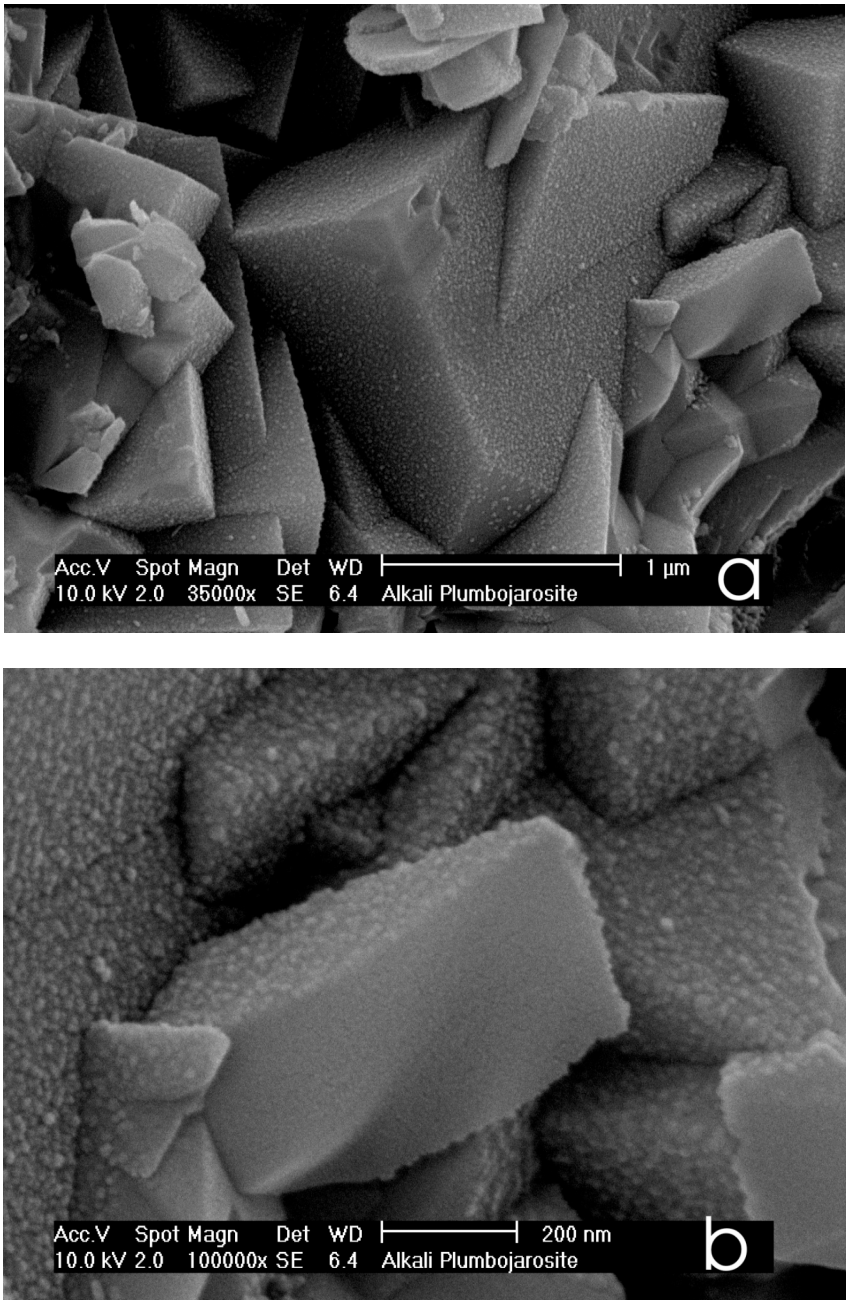

Figure 13. Scanning electron microscope (SEM) images of the residual solid from the pH 8 dissolution of Pb-jarosite. Image (a) highlights a very fine globular coating on the surface, which is more visible in the higher-resolution image (b). Operating conditions indicated on each micrograph.

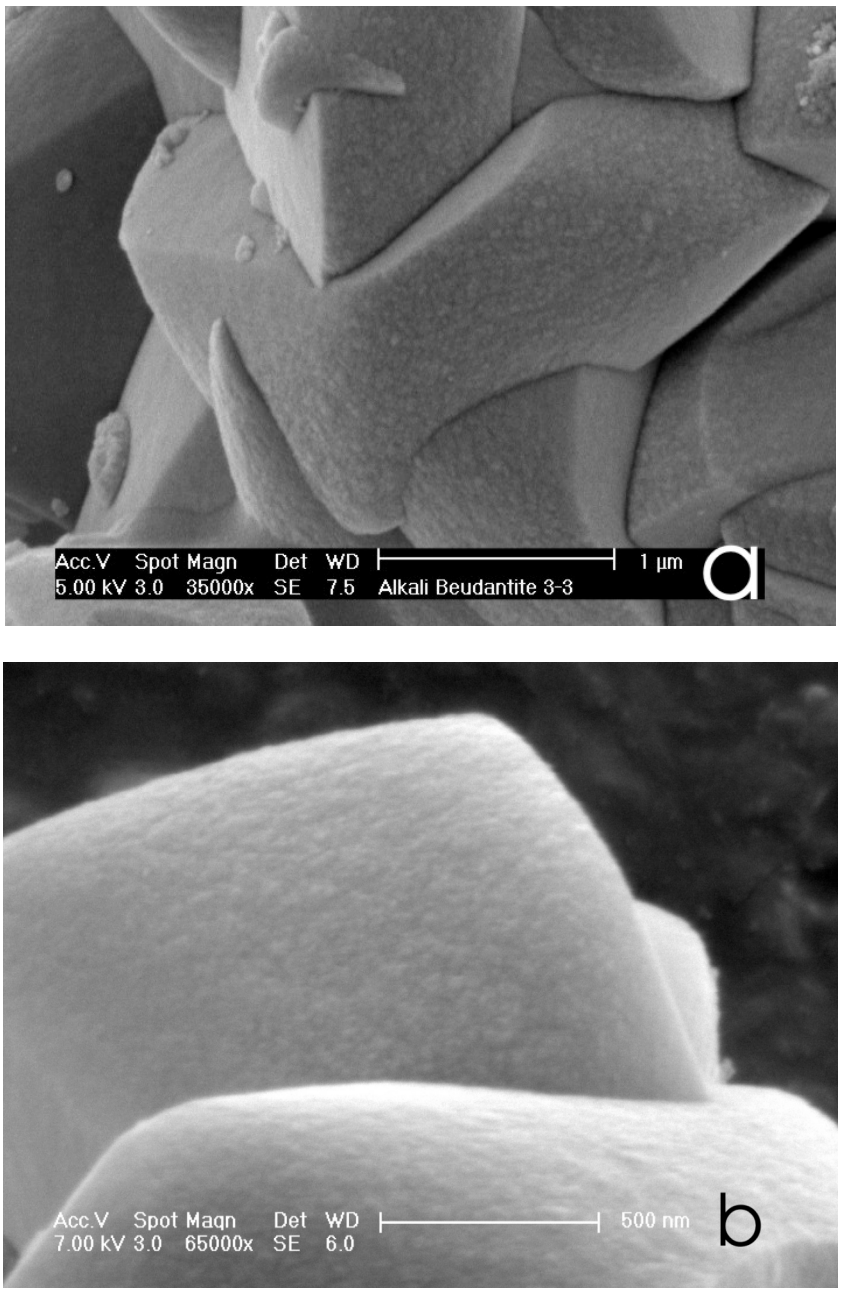

Figure 14. Scanning electron microscope (SEM) images of the residual solid from the pH 8 dissolution of Pb-As-jarosite. Image (a) highlights a very fine globular coating on the surface, which is more visible in the higher-resolution image (b). Operating conditions indicated on each micrograph.

TABLES

Table 1. Final pH and aqueous concentrations and molar ratios for Pb- and Pb-As-jarosite dissolution experiments.

Mineral	Final pH	Concentrations (mmol L^{-1})				Molar ratios			
		Pb	Fe	SO_4	AsO_4	Pb	Fe	SO_4	AsO_4
pH 2 Dissolutions									
Pb-jarosite	2.07	0.0108-0.0196	0.2797-0.4873	0.1973-0.3487	-	0.109-0.112	2.79-2.83	2	-
Pb-As-jarosite	2.10	0.000034-0.000059	0.0723-0.0735	0.0141-0.0145	0.0404-0.0416	0.0040-0.0069	8.485-8.713	1.69	4.741-4.849
pH 8 Dissolutions									
Pb-jarosite	3.44-3.54	0.0066-0.0071	0.0004	0.1194-0.1269	-	0.110-0.112	0.0063-0.0067	2	-
Pb-As-jarosite	4.58-4.78	0.00007	0.000087-0.000127	0.0135-0.0151	0.0014-0.0017	0.0078	0.0097-0.0158	1.69	0.175-0.190

Table 2. Calculated equilibrium activities.

Mineral	Final pH	log $\{SO_4^{2-}\}$	log $\{H_2AsO_4^-\}$	log $\{Pb^{2+}\}$	log $\{Fe^{3+}\}$	Charge balance error (%)	Calculated log IAP
pH 2 Dissolution							
Pb-jarosite	2.07	-3.85--4.09	-	-4.96--5.21	-3.87--4.10	3-5	-9.35±0.25--10.65±0.25
Pb-As-jarosite	2.10	-5.20--5.21	-4.78--4.80	-7.47--7.70	-4.67	5	-

Table 3. Calculated saturation indices for pH 2 dissolutions.

Mineral	Saturation Indices (log Q/K)*
pH 2 Dissolution	
Pb-jarosite	Hematite 4.13-4.59 Goethite 1.58-1.82 Anglesite -0.96-(-1.45)
Pb-As-jarosite	Hematite 3.12-3.15 Goethite 1.08-1.09

* Only minerals with log Q/K > -3 are listed

Table 4. Residual solid concentrations and molar ratios for Pb- and Pb-As-jarosite dissolution experiments.

	Concentrations (mmol L^{-1})				Molar Ratios			
Mineral	Pb	Fe	SO_4	AsO_4	Pb	Fe	SO_4	AsO_4
pH 2 Dissolutions								
Pb-jarosite	0.0273-0.0276	0.3628-0.3723	0.2306-0.2376	-	0.230-0.236	3.133-3.147	2	-
Pb-As-jarosite	0.0920-0.0927	0.6660-0.6754	0.3590-0.3643	0.0335-0.0341	0.430-0.433	3.129-3.135	1.69	0.157-0.160
pH 8 Dissolutions								
Pb-jarosite	0.0355-0.0366	0.7267-0.7323	0.3987-0.4012	-	0.178-0.183	3.639-3.673	2	-
Pb-As-jarosite	0.0844-0.0855	0.6949-0.7041	0.3458-0.3497	0.0549-0.0556	0.412-0.415	3.396-3.412	1.69	0.267-0.270

Table 5. Percentage of ions released from dissolved solids into solution

	% ions released from solid to solution			
Mineral	Pb	Fe	SO_4	AsO_4
pH 2 Dissolutions				
Pb-jarosite	4.14-7.52	4.77-8.32	4.92-8.69	-
Pb-As-jarosite	<1	1.38-1.41	<1	7.13-7.34
pH 8 Dissolutions				
Pb-jarosite	2.53-2.72	<1	2.98-3.16	-
Pb-As-jarosite	<1	<1	<1	<1